AD-A256 397

REPORT DOCUMENTATION PA

DTIC
ELECTE
OCT 13 1992
S C D

ved
04-0188

1a. REPORT SECURITY CLASSIFICATION UNCLASSIFIED	1b. R

2a. SECURITY CLASSIFICATION AUTHORITY

2b. DECLASSIFICATION / DOWNGRADING SCHEDULE

3. DISTRIBUTION / AVAILABILITY OF REPORT
Approved for public release; distribution is unlimited.

4. PERFORMING ORGANIZATION REPORT NUMBER(S)
SESC-UAPB-01-92

5. MONITORING ORGANIZATION REPORT NUMBER(S)
AFOSR-TR. 02 0007

6a. NAME OF PERFORMING ORGANIZATION Univ of Arkansas/Pine Bluff	6b. OFFICE SYMBOL (If applicable)	7a. NAME OF MONITORING ORGANIZATION AFOSR/NL

6c. ADDRESS (City, State, and ZIP Code) Pine Bluff, AR 71601	7b. ADDRESS (City, State, and ZIP Code) Building 410, Bolling AFB DC 20332-6448

8a. NAME OF FUNDING / SPONSORING ORGANIZATION AFOSR	8b. OFFICE SYMBOL (If applicable) NL	9. PROCUREMENT INSTRUMENT IDENTIFICATION NUMBER F49620-89-C-0071

8c. ADDRESS (City, State, and ZIP Code)
Building 410, Bolling AFB DC
20332-6448

10. SOURCE OF FUNDING NUMBERS

PROGRAM ELEMENT NO.	PROJECT NO.	TASK NO.	WORK UNIT ACCESSION NO.
61102F	2310	A2	

11. TITLE (Include Security Classification)
(U) Global Zones of Particle Precipitation as observed by EXOS-C

12. PERSONAL AUTHOR(S)

13a. TYPE OF REPORT Reprint/Annual/Final	13b. TIME COVERED FROM 7/1/91 TO 6/30/92	14. DATE OF REPORT (Year, Month, Day) 92/7/27	15. PAGE COUNT 32

16. SUPPLEMENTARY NOTATION
Name of Journal and Article Number

17. COSATI CODES			18. SUBJECT TERMS (Continue on reverse if necessary and identify by block number)
FIELD	GROUP	SUB-GROUP	

19. ABSTRACT (Continue on reverse if necessary and identify by block number)
A study of the temporal variation of quasi-trapped proton population near the geomagnetic equator reveals that the peak value of the equatorially mirroring component may increase by a factor of 50 or more between a solar maximum and a minimum conditions. During a solar maximum condition more hydrogen escape to outer space than during a minimum condition. The escaping light gas may cause more neutral generation by charge exchange interaction with the radiation belt/ring current protons, thereby enhancing the quasitrapped proton population at equatorial thermospheric altitude. This reported result is based on the observation of quasitrapped proton population in 1969-70, 1982, and 1984-86 by AZUR, S81-1, and EXOS-C missions. Also, a study based on EXOS-C mission alone shows that the peak flux profile of protons precipitated in the equatorial, and low-latitude, midlatitude, and auroral zones lying to the north of the equator, exist in parallel with the minimum magnetic field equator. Further, proton (0.64 – 35 MeV) and electron (0.19 – 3.2 MeV) population in the said midlatitude zone show longitude and altitude dependences. Contrary to previous observations, the locations of the peak flux

20. DISTRIBUTION / AVAILABILITY OF ABSTRACT ☐ UNCLASSIFIED/UNLIMITED ☐ SAME AS RPT. ☐ DTIC USERS	21. ABSTRACT SECURITY CLASSIFICATION UNCLASSIFIED
22a. NAME OF RESPONSIBLE INDIVIDUAL J. G. STORIE, LtCol, USAF	22b. TELEPHONE (Include Area Code) (202) 767-5021	22c. OFFICE SYMBOL AFOSR/NC

DD Form 1473, JUN 86 — Previous editions are obsolete. — SECURITY CLASSIFICATION OF THIS PAGE

19. Abstract cntd.

profiles in all the three zones in L space depend upon the pitch angle of the particles. Particle pitch angle distribution shows a second peak in addition to the one at 90 degrees pitch angle. Particle flux does not depend on the local time. However, there is a great relative variation in e and p fluxes detected in the study of the seasonal variation of these fluxes. Particle flux variations are indicative of the presence of scattering by electromagnetic waves generated in the ionosphere. A study of the energy spectra of p flux shows a knee at about 1 MeV. No such observation is seen in the spectra of e flux. Theoretical understanding of these observations is in progress along with the work of data analysis of other parts of the global zones.

Annual Report (1991 – 92)
for
AFOSR Contract F49620-89-C-0071

"Global Zones of Particle Precipitation as Observed by EXOS-C"

M. A. Miah, Ph. D.
Associate Professor of Physics
Space and Environmental Sciences Center
University of Arkansas at Pine Bluff
Pine Bluff, AR 71601

I. INTRODUCTION

The equatorial particle precipitation project started in 1990 was completed with the conclusion that during a solar maximum period proton population may increase by 50 or more depending on the severity as compared to that during a solar minimum period. Further, a detailed study of the instrument response function for various orientation of the telescope axis with respect to the magnetic field direction was made to reach the conclusion. Later, efforts were directed to study the off-equatorial zones of particle precipitation. It was found that the global peak flux profiles exist in parallel with the minimum magnetic field equator.

A broader study of the midlatitude zone to the north of the equator reveals, contrary to previous reports, that the locations of the peaks of e and p fluxes in L space are dependent upon the particle pitch angles. The fluxes also show both altitude and longitude dependences. Local time does not influence the particle fluxes. However, they show seasonal dependences. Energy spectra of p flux show a knee at ~ 1 MeV. No such observation is found in e flux. Theoretical understanding of these observations are on-going along with the analysis of data from the rest of global zones.

About the presentations and publications made, a paper titled "Spatial and Temporal Variation of 0.65 – 35 MeV Protons and 0.19 – 3.2 MeV electrons in the Space Station Environment" has been published in the Journal of Geomagnetism and Geoelectricity. Another paper titled "Solar-induced Variation of Proton Precipitation Near the Equator" has just been revised and mailed to the US Editor of the Journal of Atmospheric and Terrestrial Physics (JATP) for publication. A third paper titled "Solar Cycle Dependence of Proton Population Near the Equator" was submitted for publication in the proceedings of Solar-Terrestrial Relationship Workshop held in May, 1992, in Ottawa, Canada. Prior to this Workshop,

92 10 9 057

an abstract on equatorial particle precipitation was submitted to American Geophysical Union (AGU) for presentation in the Joint Spring meeting held in Montreal. Further, a fourth paper on the topic of spatial and temporal features of protons and electrons in the low- and mid-latitude zones was presented in the Western Pacific Geophysics meeting in Hong Kong during August 16 - 21, 1992. Recently, a fifth paper titled "Significant Variation of Proton Population Near the Equator" was presented in the World Space Congress meeting in Washington, DC, during August 28 - September 7, 1992. The paper is still in the review process for consideration of publication in COSPAR journal.

Briefly, the work accomplished during the 1991-92 period is described below.

II. TEMPORAL VARIATION OF PROTONS FLUX IN THE EQUATORIAL ZONE

The study of the equatorial zone was completed with the conclusion of enormous variation of proton flux with the solar maximum and minimum conditions. The energy range of protons under study extends from the energy of quasi-trapped to stably trapped protons. Some reasoning has been used to estimate the fraction of quasi-trapped protons in that energy range. Further, in order to know the energy spectra and the mean energy we have to compare our data with observations made at both the low and high energy ends of the energy range in the comparable altitude and L ranges near the equator. We take help of the observations at the low energy end by Mizera and Blake (1973), Hovestadt et. al. (1872), Moritz (1972), and Scholer et. al. (1975), and at the high energy end by Fischer, et. al. (1977), Claffin and White (1974), and Parsignault et. al. (1981).

II. A. Quasi-trapped Component

In Fig. 1, we have compiled the data of both low and high energy protons from the previous observations. We have covered the energy range of less than 10 keV to 35 MeV comprising poststorm, prestorm, and averge geomagnetic conditions. Dial data (Fischer et. al., 1977) are represented by the three curves to the right side beyond 5 MeV corresponding to, from the bottom, L=1.15, 1.18, and 1.20. EXOS-C data are plotted at 9.53 MeV by five horizontal lines corresponding to, from the bottom, L=0.98, 1.02, 1.08, 1.14, and 1.18. The other two horizontal lines at 1.3 MeV are from Phoenix-1 observation (Miah, 1989, 1991b, 1991c, 1992), the bottom line is the observed flux at 277 km and the top line for the extrapolated flux at 450 km based on the altitude dependence of observation. The equatorial perpendicular peak flux of protons shows an L dependence of $\sim L^{81}$ (Fischer et.
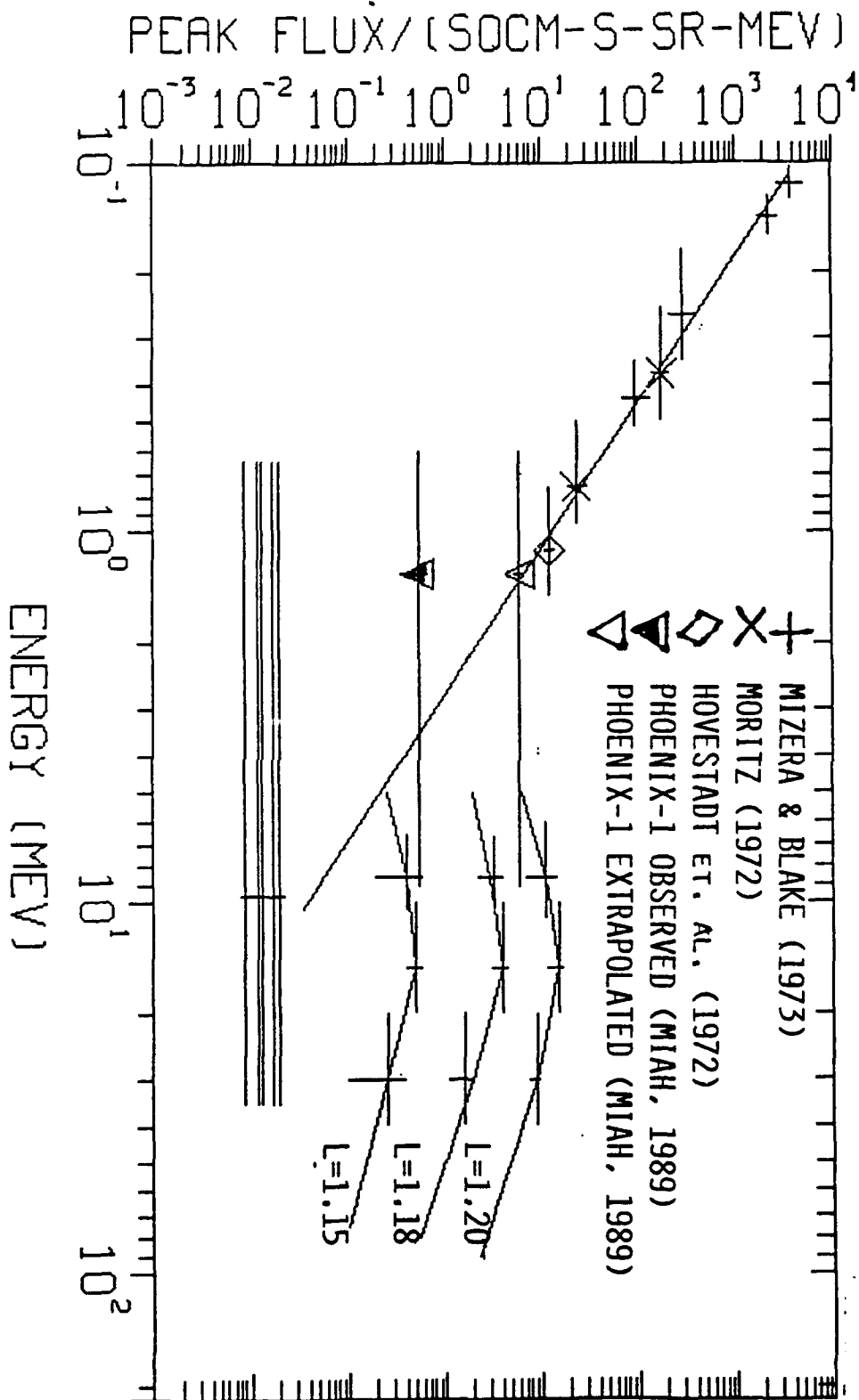
PEAK FLUX/(SOCM-S-SR-MEV)

10^{-3} 10^{-2} 10^{-1} 10^{0} 10^{1} 10^{2} 10^{3} 10^{4}

10^{-1} 10^{0} 10^{1} 10^{2}

ENERGY (MEV)

Figure 1

+ MIZERA & BLAKE (1973)
X MORITZ (1972)
◇ HOVESTADT ET. AL. (1972)
◀ PHOENIX-1 OBSERVED (MIAH, 1989)
◁ PHOENIX-1 EXTRAPOLATED (MIAH, 1989)

L=1.15
L=1.18
L=1.20

al., 1977; Claffin and White, 1974) in the energy range of ~ 5 MeV to beyond the higher energy end of the S-1 integral energy channel. The L dependence of S-1 measured perpendicular peak flux of protons is only $L^{4.25}$ as has been reported above. The very low power law index of 4.25 compared to the large index of 81 indicates that the portion of higher energy component of protons in the flux is negligible compared to the lower energy quasi-trapped component. The next subsection estimates it to be nearly one-quarter of the low energy population, if 5 MeV (based on available measurements) is taken as the upper limit of the low energy component.

II. B. Mean Energy of the Protons

Following the observations of L independence of low energy particles (Moritz, 1972; Miah, 1992), we have plotted the low energy (10 keV < E < 2 MeV) equatorial flux in the L range of 0.98 to 1.14. A least square fit to the data describes the flux by the power law of exponent -2.55 (Miah, 1989, 1991b, 1991c, 1992). Without any anticipation of abrupt changes, we assume the power law $E^{-2.55}$ to be valid at L=1.15 for low energy protons up to 5 MeV. This inclusion does not affect the integral energy flux significantly because of the steep nature of the curve. In the wide energy range of observation, Dial (Fischer et al., 1977) data at L=1.15 fits $E^{0.4}$ for $5 \leq E \leq 15$ MeV and $E^{-1.0}$ for $15 \leq E \leq 35$ MeV. At this L shell, the proportion of the integral energy fluxes in the three intervals are shown in Table 1 below.

TABLE 1

Energy Rangewise Integral Energy Flux

Energy interval (MeV)	Power Law	Flux (cm^{-2}-sr^{-1}-s^{-1})
0.64 - 5.0	$E^{-2.55}$	16.00
5.0 - 15.0	$E^{0.4}$	4.22
15.0 - 35.0	$E^{-1.0}$	2.70

The integral energy flux observed by EXOS-C at L = 1.15 is 0.62 $cm^{-2}s^{-1}sr^{-1}$ The proportions shown in Table 1 yields 0.433 cm^{-2}-s^{-1}-sr^{-1} in the range 0.64 to 5 MeV, 0.114 cm^{-2}-s^{-1}-sr^{-1} in 5 to 15 MeV, and 0.073 cm^{-2}-s^{-1}-sr^{-1} in 15 to 35 MeV. The mean energy of the protons as determined from the integration of the weighted normalized power laws in the three different regions was found to be 9.53 MeV. The bottom four horizontal lines are drawn with the full energy range of the EXOS-C energy channel. For comparison, normalized $E^{-2.55}$ law alone yields the mean energy to be 5.69 MeV.

II. C. Flux Discrepancy

A striking point in the plot is the low value of the flux observed in the S-1 telescope. This flux is 27.8 times lower than the power law predicted value ($0.64 \leq E \leq 35$ MeV), 7.7 times lower than the Phoenix-1 (Miah et. al., 1988; Miah, 1989; 1991b, 1991c, 1992) observed flux ($0.6 \leq E \leq 9.1$ MeV) at 277 km, and 87.7 times lower than the Phoenix-1 extrapolated flux at 450 km. The flux (cm^{-2}-sr^{-1}-s^{-1}) comparison is shown in Table 2.

Table 2

Comparison of Flux

Power law predicted	Phoenix-1 Observed at 277 km	Phoenix-1 Extrapolated to 450 km	EXOS-C Observed
16.7	4.64	52.7	0.60

The actual flux comparison needs involvement of the instrument response functions which are not the same for all the telescopes at the geomagnetic equator. We postpone the explanation of this flux decrease in 1984-86 until we have compared absolute fluxes during the epochs of observation in 1982 and 1984-86.

II. D. Instrument Response Function

The study of temporal variation with the same instrument at different times is much easier than that when the comparison involves between measurements made by different instruments because of the messy calculation of the response function of the instrument to particles of different pitch angles. We calculate the changes of absolute flux between the epochs of 1982 when the sun was very violent and 1984-86 when the sun passes through a solar minimum. The particle counting rate R of a detector of area A having efficiency function $f(\alpha)$ between the energy range E_1 and E_2 for the spectrum $E^{-\delta}$, and the pitch angle range α_1 to α_2 for the pitch angle distribution characterized by $\sin^q \alpha$ at the magnetic field B, magnetic shell L, latitude λ, longitude ϕ, and time t is given by (Miah, 1990, 1991)

$$R = 1/T \int_0^T dt \int_{E_1}^{E_2} dE \ E^{-\delta} \int_\Omega d\omega \int_A dA \cdot r(\omega) \ J_n(B, L, \lambda, \phi, q, t) \qquad (1)$$

To evaluate the integral numerically, we split it into parts which yield

$$R = A \ F \ J_n \ Q \qquad\qquad (2)$$

In eqn. (2)

$$F = \int_{\alpha_1}^{\alpha_2} \sin^q\alpha \ f(\alpha) \ d\alpha \qquad\qquad (3)$$

and

$$Q = \int_{E_1}^{E_2} E^{-\delta} \ dE \qquad\qquad (4)$$

The efficiency function $f(\alpha)$ can be evaluated for the telescopes (Miah, et. al., 1989). For illustration, the efficiency functions of all three telescopes in AZUR, S81-1, and EXOS-C have been plotted in Figure 2. AZUR telescope has the smallest efficiency function in the smallest equatorial pitch angle range. The next one is the S-1 telescope on board EXOS-C. The Monitor telescope in the Phoenix-1 experiment on board the S81-1 mission has the largest efficiency and largest equatorial pitch angle range. The efficiency functions plotted are relative to 2π, the efficiency function of a plane detector. Sine function raised to some exponents can be used to fit the efficiency functions. Taking a range of exponents for the pitch angle distribution function, Eqn. (3) can be evaluated numerically. Eqn. (2) lets us calculate J_n from the counting rates, detector area, integral of the product functions of pitch angle distributin, the response function, and the integral spectrum. From eqn. (2), the normalization constant J_n which is representative of the actual flux, can be calculated.

We have plotted the instrument response function of the S-1 telescope on board EXOS-C for several orientation of the telescope axis with respect to the magnetic field direction, i. e. for different values of the angle χ. Later part of the report will refer to these plots. Figs. 3a through 3f illustrate the instrument efficiency functions. While no direct relation between the counting rates and the efficiency function is illustrated here, the figures distinctly show that between the efficiency function and the angle χ.

II. E. Comparison of Absolute Flux

For comparison of absolute fluxes, we have plotted J_n in

Figure 2

ANGLE BETWEEN SI-AXIS AND B-VECTOR -90

RESPONSE FUNCTION

PITCH ANGLES (DEG)

SOLID LINE 80 (DEG)

$X = 100°$

70 (DEG)

$X = 110°$
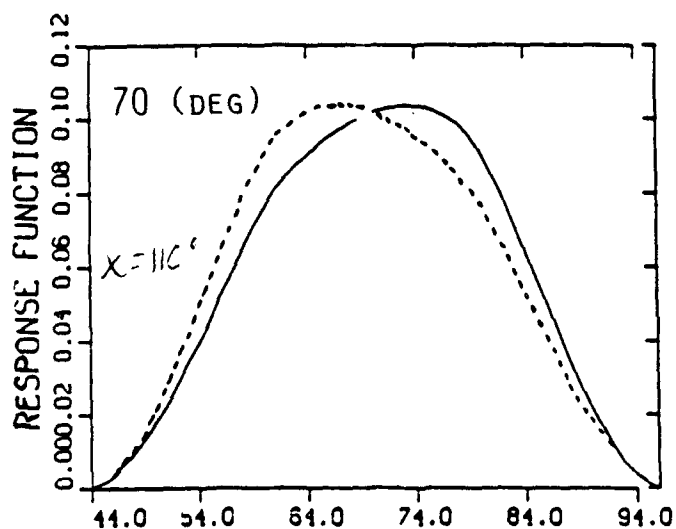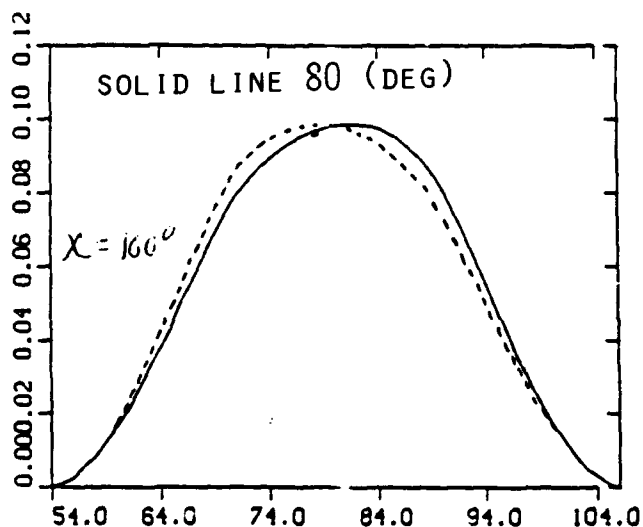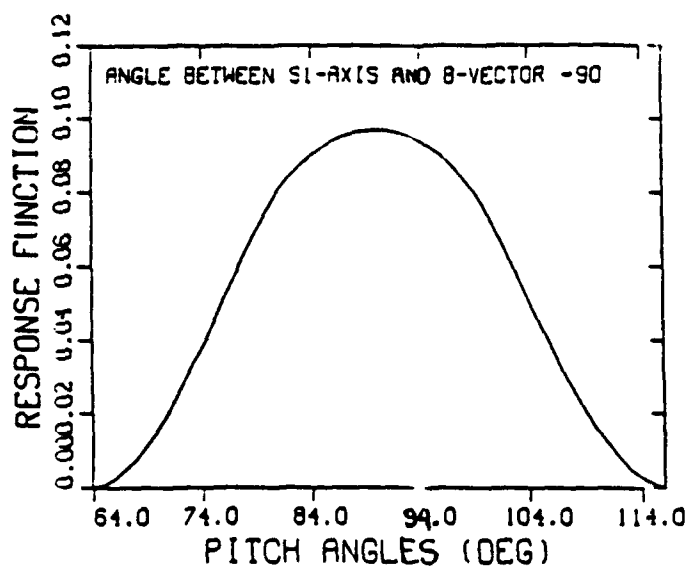
60 (DEG)

$X = 120°$

50 (DEG)

$X = 130°$

40 (DEG)

$X = 140°$
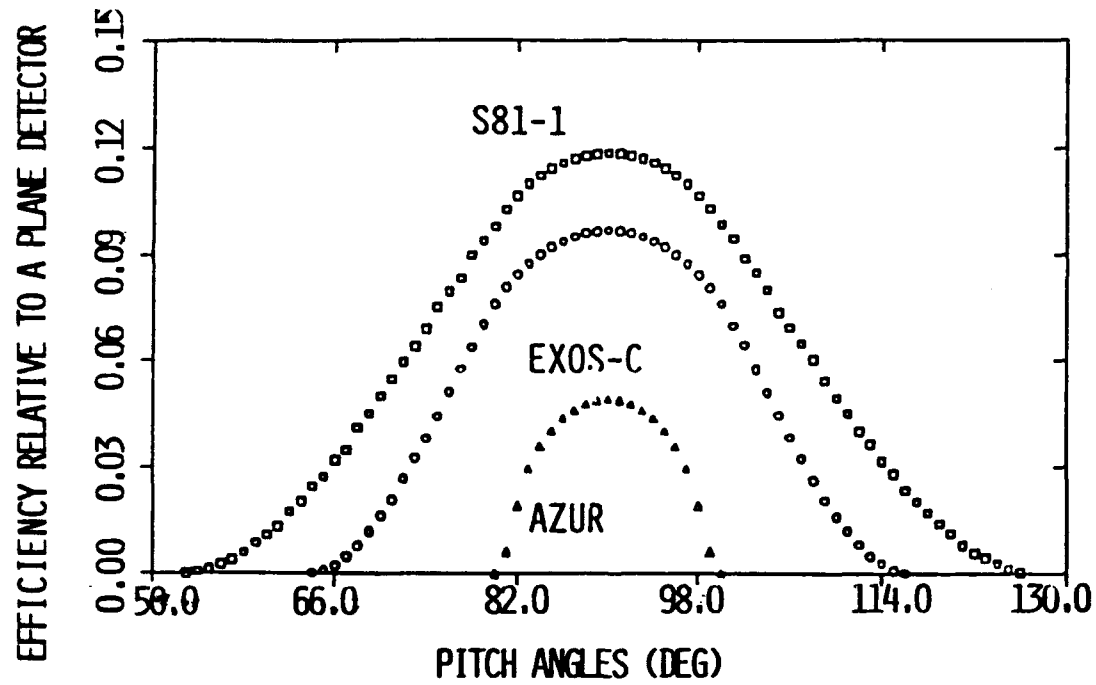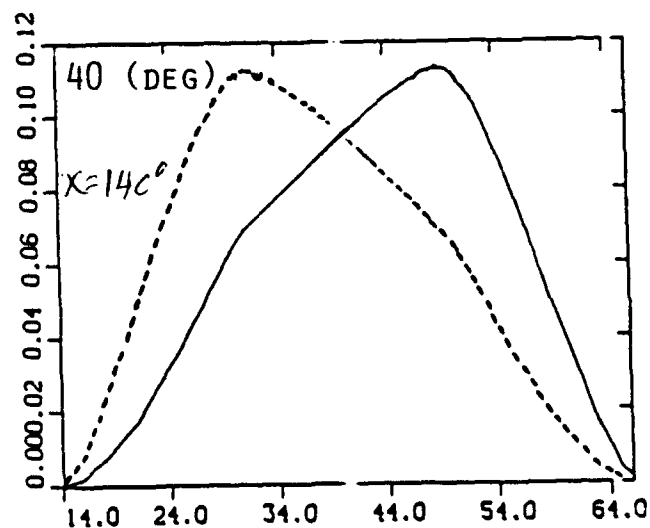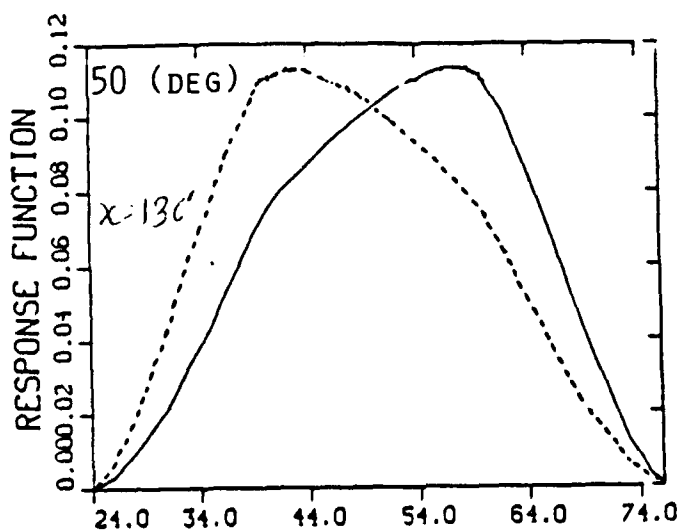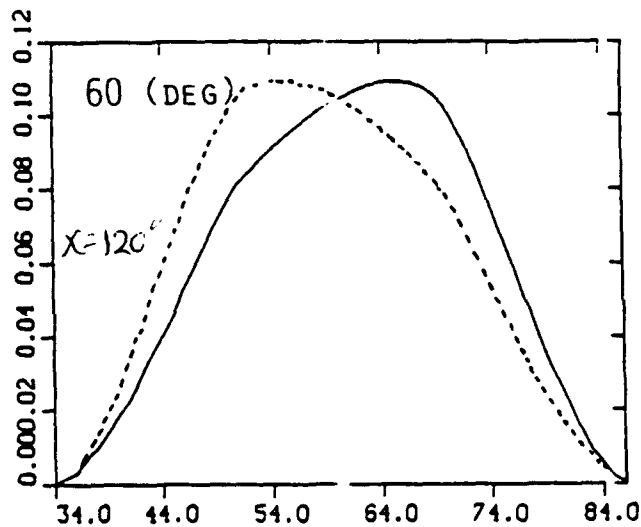
Figur 3a through 3f. Plots of response functions vs pitch angle fordifferet
orientations of the telescope axis with respect to the magnetic field direction.
This angle has been designated by Xi. Xi values are gradually decreasing for the
solid curves from 90 to 40 degrees, and increasing for dotted curves from 90° – 140°.

Fig. 4 for the known values of q. The dependences of J_n upon other variables are not significant (Miah, 1989, 1991b). The bottom curve marked with circles is for EXOS-C observation. The second curve from the bottom marked with triangles is AZUR's observation. The third curve marked by plus signs is Phoenix-1 data. The fourth curve marked by crosses is the Phoenix-1 data predicted by the source depletion model (Miah, 1989, 1991b, 1991c, 1992). The top curve marked by squares is Phoenix-1 data extrapolated to 450 km. EXOS-C observation is 39.5, 39.6, 59.4, 420.5 times less than AZUR, Phoenix-1 observed, Phoenix-1 predicted by source depletion, and Phoenix-1 extrapolated flux, respectively. Fig. 4, in essence, compares the absolute population of quasi-trapped in the equatorial thermosphere.

II. F. Impact of Solar Conditions

The fact that the absolute flux in 1984-86 is 40 times less than that in 1982 (Miah, 1991b) or that in 1969-70 (Moritz, 1972) warrants our special attention. We have seen in Eqn. (2) that J_n remains to be a function of t, i. e epoch. The large variation is, probably, because of the solar condition. The sun was passing through a maximum condition in 1982 and a minimum in 1984-86 as shown in Fig. 5 (Coffey, 1992). During the solar maximum condition, the radiation belt particle intensity increases. Further, light gases escapes to exosphere more during the maximum conditions as shown in Fig. 6 (Fahr and Shizgal, 1983). More hydrogen escapes cause more precipitation of low energy particles. Also, the depression of thermosphere toward the Earth may cause generation of more quasi-trapped particles at low altitude in 1982. The average solar 10.7 cm radio flux during 1984-86 was ~ 80 and in 1982 was ~ 175 (NOAA, 1987). The exospheric temperature corresponding to these solar inputs were ~ 750°K in 1984-86 and ~ 1140° K in 1982 (Jacchia, 1977). The Jeans hydrogen escape fluxes (Fahr, and Shizgal, 1983), corresponding to these temperatures, are ~ 28 in 1984-86 and ~ 750 in 1982. Since majority of the observed particles are of the low energy region where charge exchange production predominates, it is likely that upward escaping gases enhanced the neutral generation, and consequently, increased low altitude flux in 1982, or decreased the flux in 1984-86.

III. LOW- AND MID-LATITUDE ZONE DATA PROCESSING/ANALYSIS

Previously developed software was revised and some new software was developed, tested, and applied to decode the data of both the differential and integral proton and electron channels, pertaining to the low latitude, midlatitude, and auroral zones lying to the northern part of the geomagnetic
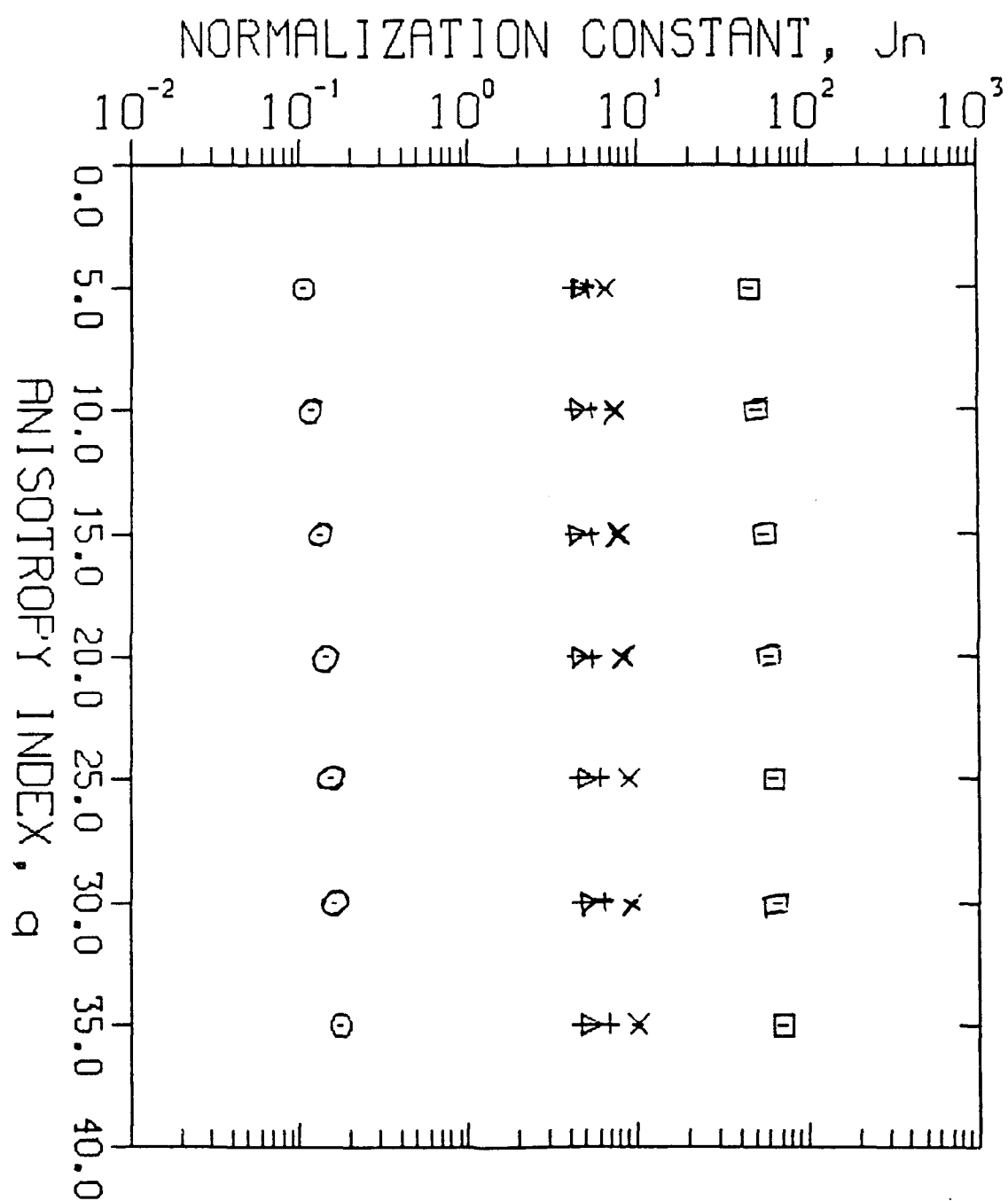
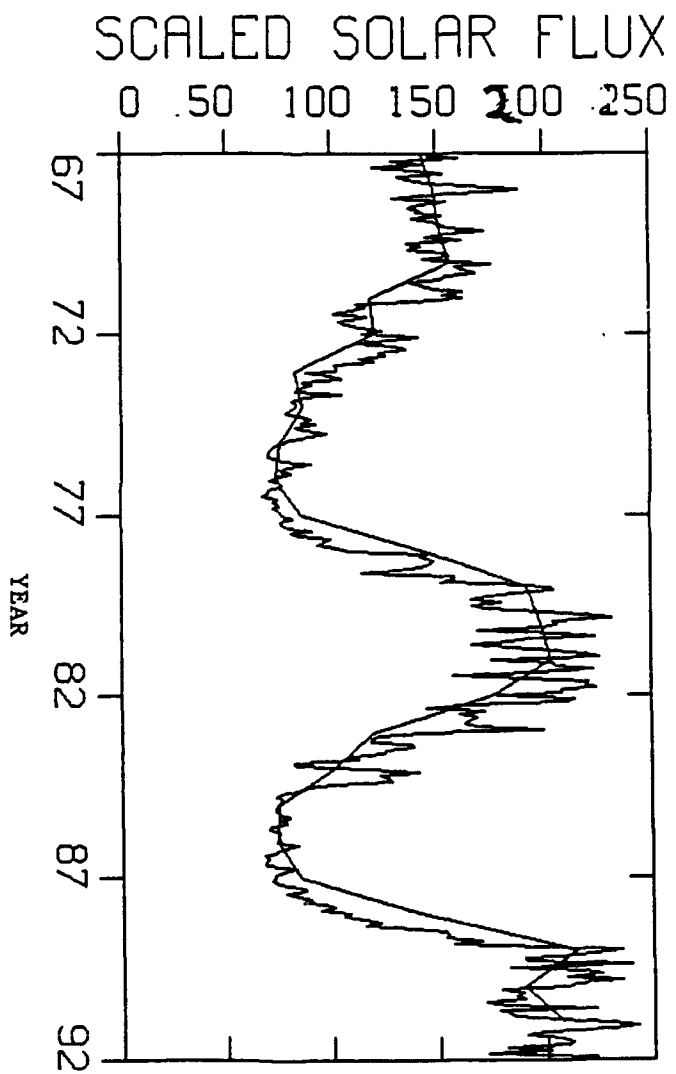NORMALIZATION CONSTANT, Jn

Figure 4

SCALED SOLAR FLUX

YEAR

Figure 5

Monthly (overshoots and undershoots) and annual (smooth) average values have been plotted
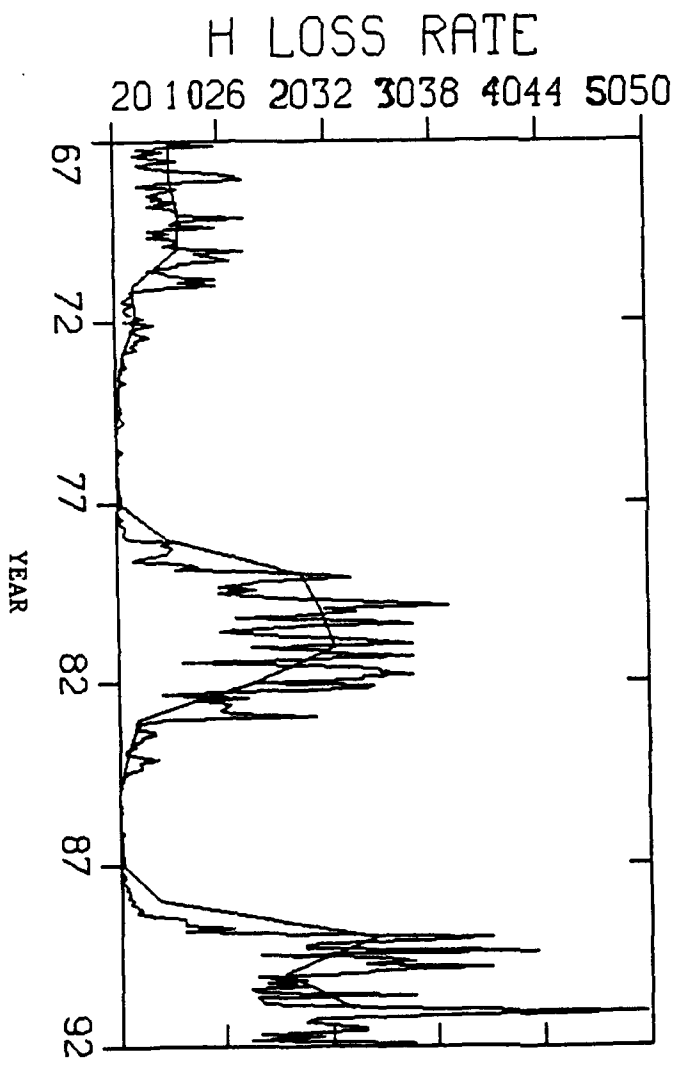
Figure 6. Monthly and annual average values have been plotted. Smooth lines are annual values.

H LOSS RATE

equator. The data were then cleaned of contaminations, especially, for rate spikes. Most part of time was devoted for the midlatitude zone e and p data. Some features of low latitude zone have also been studied. No study was made with the auroral zone.

III. A. Spatial Features

Survey Plots-. The rate spikes were detected by making plots for individual satellite passes of the average counting rates per 1° latitude bins vs latitude, longitude, altitude, L, B, local time, and the angle between the telescope axis and the magnetic field direction (χ). Figs. 7a and 7b show such plots. In these figures, the quantities along the horizontal axis are also the average values over 1° latitude bin. The zero values along this axis are to be ignored. They simply indicate the terminating position for the given pass number. The broken lines indicate protons and the solid lines electrons. Counted from the left hand side, the first peak is for the low latitude region, the second for the midlatitude region, and the third for the auroral region. These plots have helped (i) to identify the magnitudes and locations (in all the parameters along the horizontal axis) of the peak counting rates, (ii) to identify the peaks and extent of the respective regions, and (iii) to discard the data for a particular region for a given pass if contaminated by rate spikes.

Global Profile-. Global peak flux profile of protons in the three zones are shown in Fig. 8a (top). This figure shows distinctly the plots of the latitude vs longitude of the locations of the peak counting rates. Fig. 8b (bottom) shows the global profile of the minimum magnetic field equator. It is evident that the proton peak flux profiles in the three zones run parallel to the minimum magnetic field profile.

Location of Peak Counting Rates in Latitude and χ Space-. Fig. 9a shows the distribution of the peak counting rates in latitude an χ, and Fig. 9b, that in B-L space for midlatitude protons only. The top plot helps to find the latitude ranges of locally mirroring protons in all the three zones. The maximum detection efficiency of the telescope for locally mirroring particles corresponds to $\chi = 90°$ as shown in Fig. 3a above.
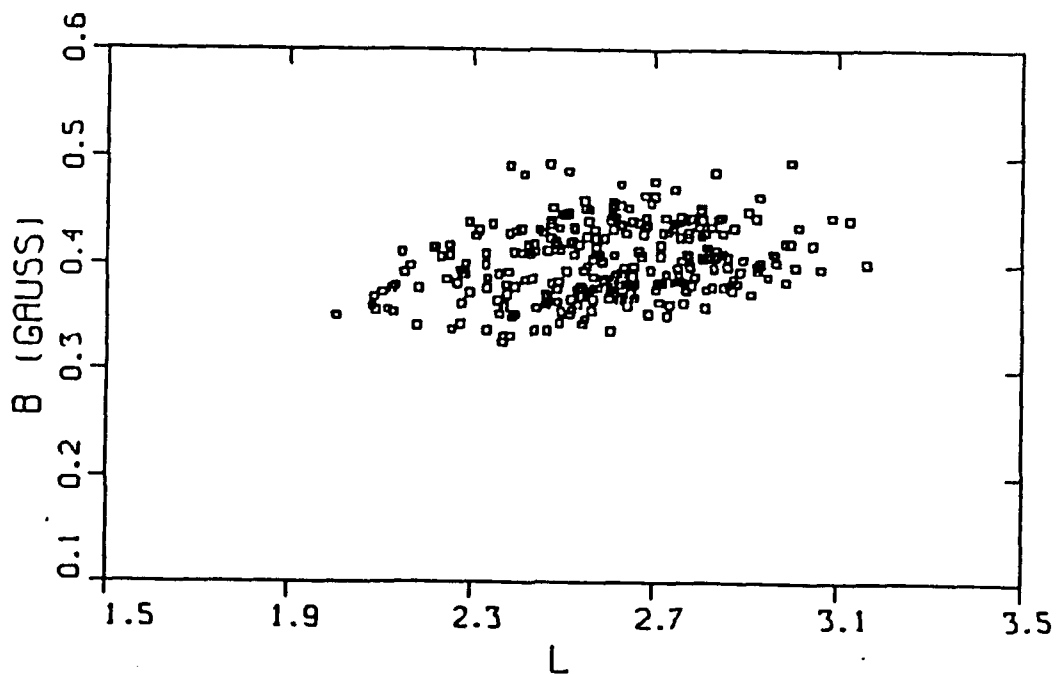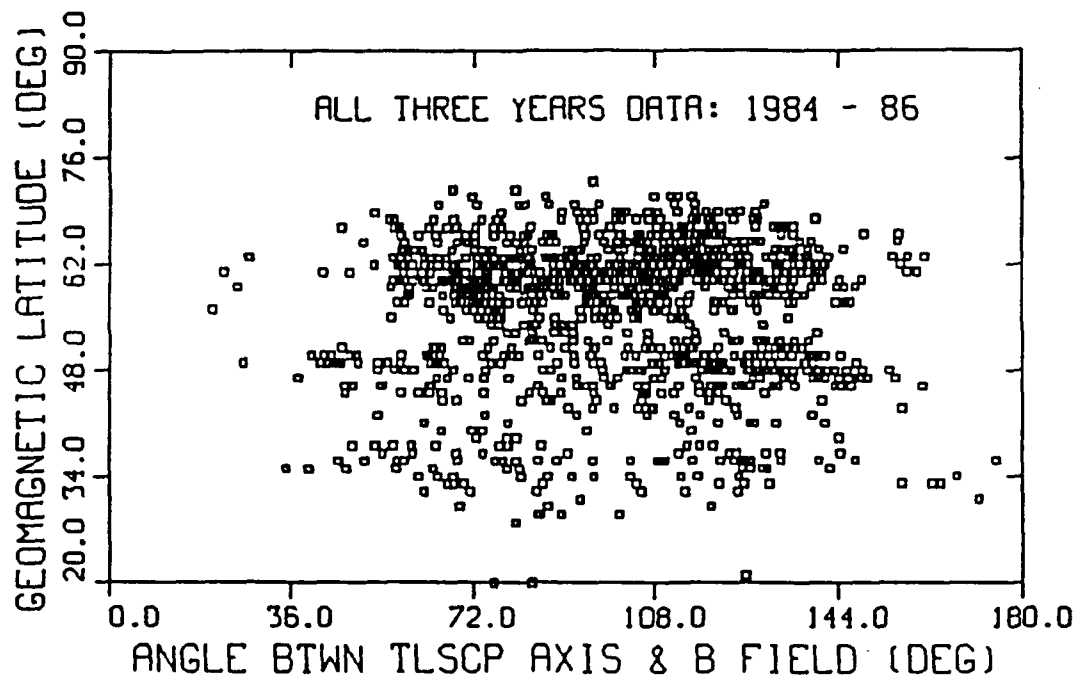
Peak Counting Rates vs χ. It was mentioned in the last year's report that a plot of the peak counting rates vs χ should look similar to the local pitch angle distribution function. Fig. 10 shows such a plot both for proton and electrons in the midlatitude zone. The plots show that the locally mirroring particles outnumber particles of other pitch angles. The second peaks in the counting rates for $70° < \chi <$
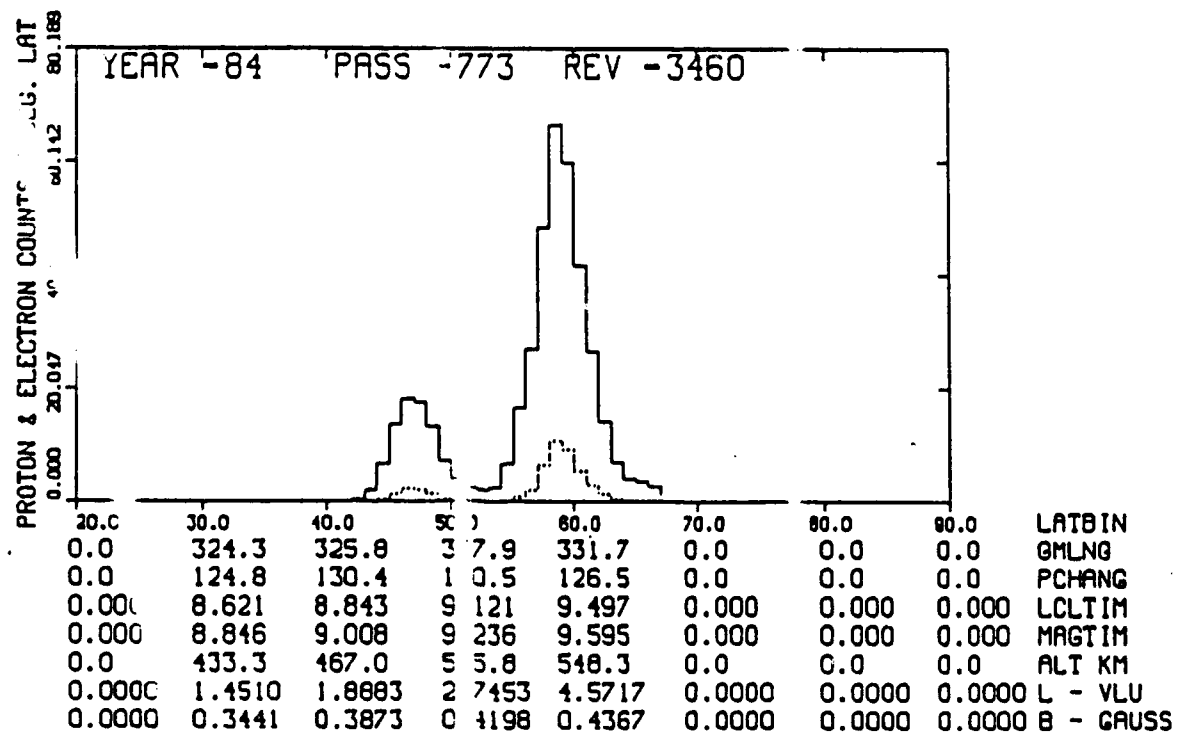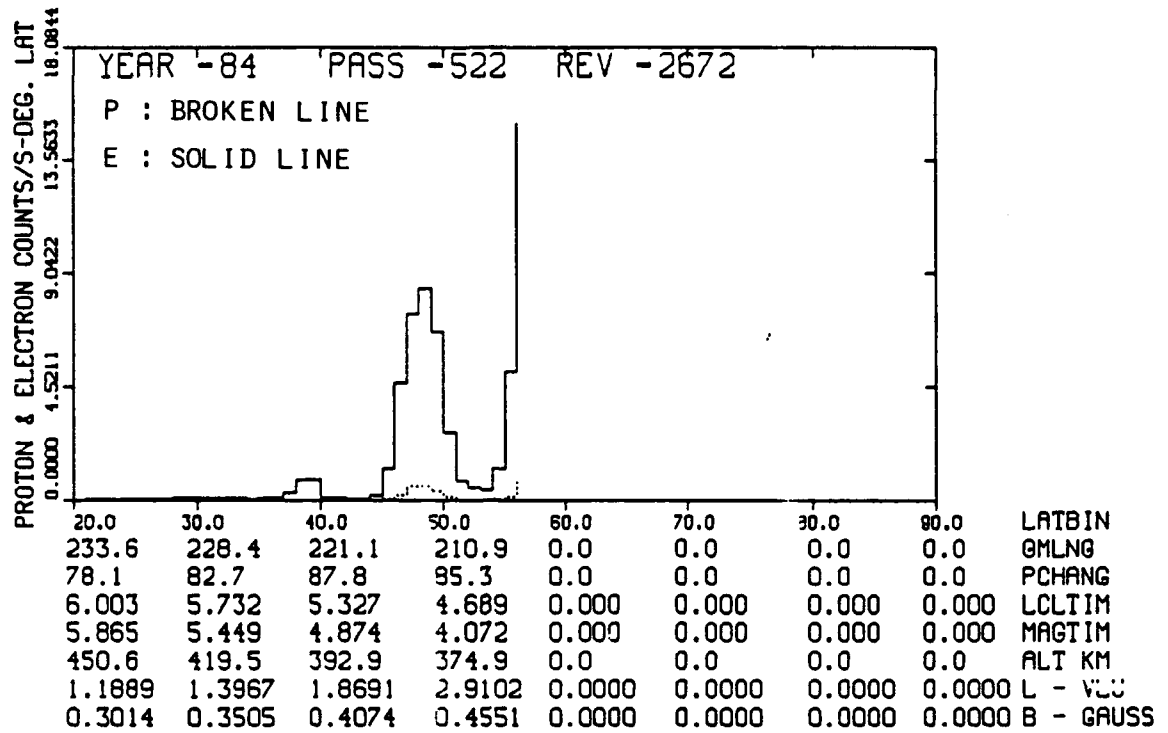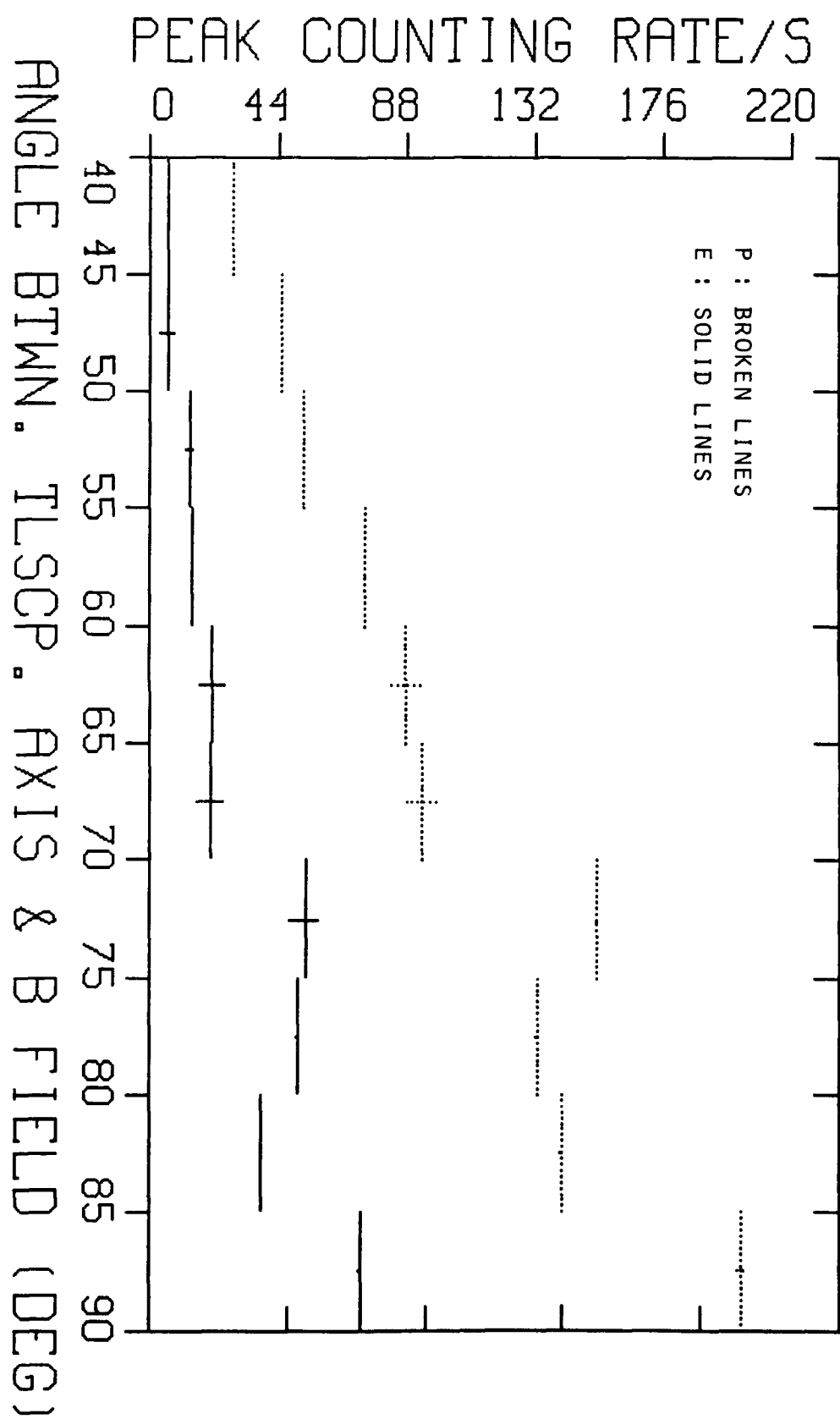
Figures 7a and 7b
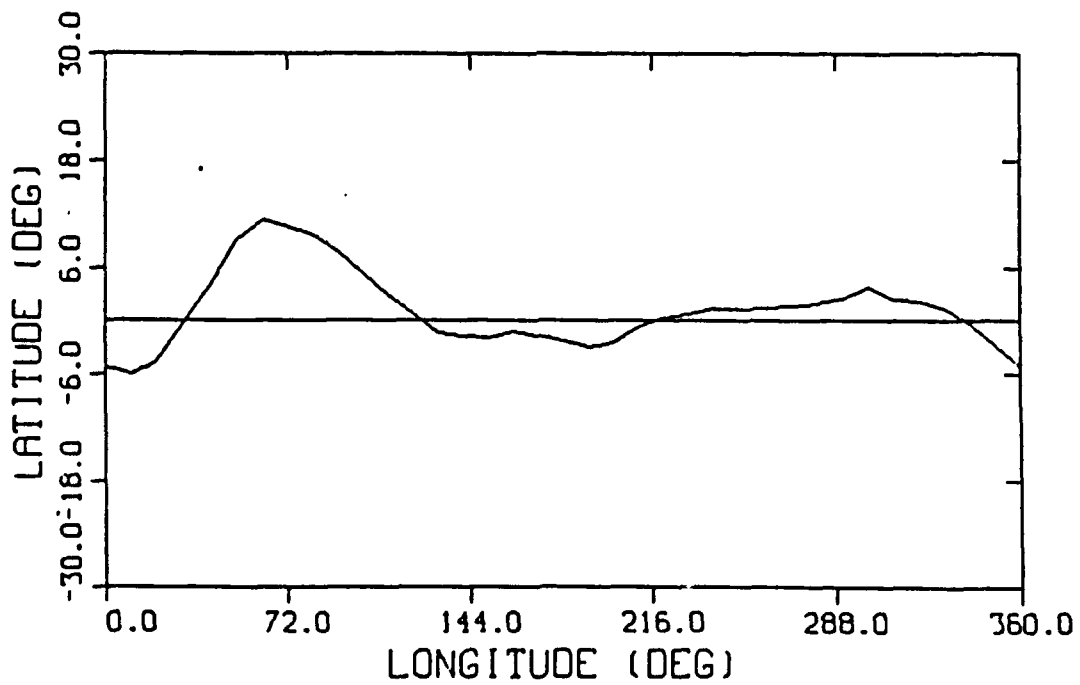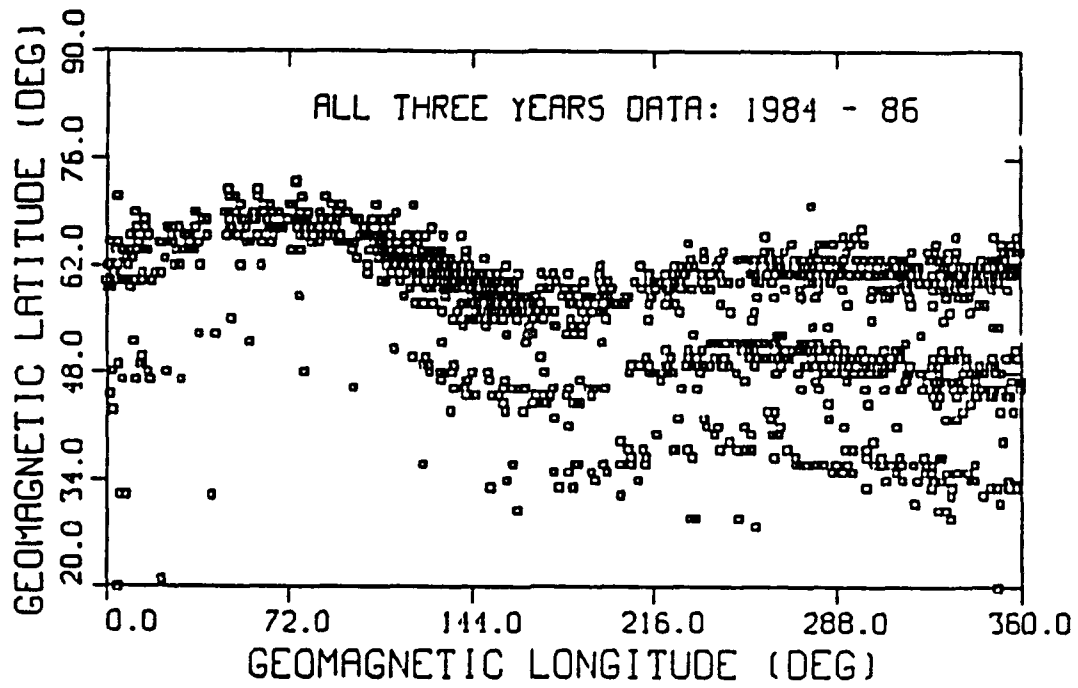
Figurs 8a and 8b

Figures 9a and 9b

Figur 10

PEAK COUNTING RATE/S

ANGLE BTWN. TLSCP. AXIS & B FIELD (DEG)

P : BROKEN LINES
E : SOLID LINES

17

80° is thought to be due to the scattering by electromagnetic waves generated in the ionosphere.

L Dependence-. The most time-consuming task was to study the L dependence of the peak flux of protons and electrons. The L range along the horizontal axis covers both the low latitude and the midlatitude. Contrary to the reports found in the literature, it is found that L dependence is dominated by the local pitch angles of the particles. This should be obvious because of the scattering effect by the electromagnetic waves generated in the ionosphere. Figs. 11 through 15 shows plots of the peak flux vs L. As said above, the dotted lines represent electrons, and the solid lines protons. Fig. 11a shows that for $85° \leq \chi \leq 90°$, in the low latitude region electron peak lies between L = 2 - 2.2, whereas proton peak between L = 1.8 - 2.0. Further, in the midlatitude region, proton peaks between L = 2.2 - 2.4, and a second electron peak is not found before L = 3 - 3.2, which is thought to fall in the auroral region. It may be that some temporal effect has masked the electron peak in the midlatitude region. Many such features are reflected in the plots through Figs. 15b.

Altitude Dependence-. Figure 16a shows altitude dependence. There is a peak value between 650 km $\leq h \leq 700$ km. The bottom figure (Fig. 16b) shows the plot of χ vs altitude. It shows that in this altitude range the χ value is far away from χ corresponding to the maximum efficiency of the telescope. This feature needs to be investigated further.

Longitude Dependence-. Figure 17a shows the longitude dependence. The drop in the flux of both electrons and protons around 30° - 72° longitude bin is due to a few data points which is evident from the bottom diagram (Fig. 17b). Within 140° - 360°, longitude dependence is virtually absent.

III. B. Temporal Features

An interesting effect is observed if we compare figures 7a and 7b with figures 18a and 18b. Again, the zeros along the horizontal axis are to be ignored. The first set of figures shows that proton counting rates are much lower than the electron counting rates. The second set of figures show the opposite effect. Differences in longitudes cannot be a reason for the variation of counting rates. Either temporal or altitude variation or both factors may contribute to this effect. However, before any conclusion can be drawn, the counting rates need to be expressed in differential flux.
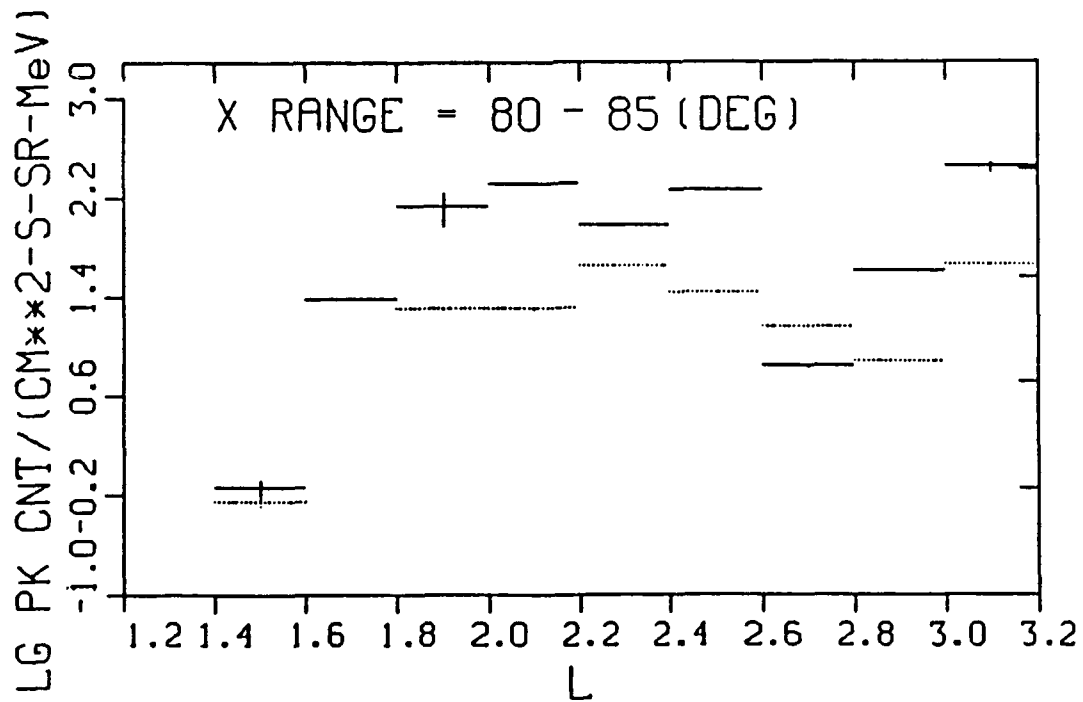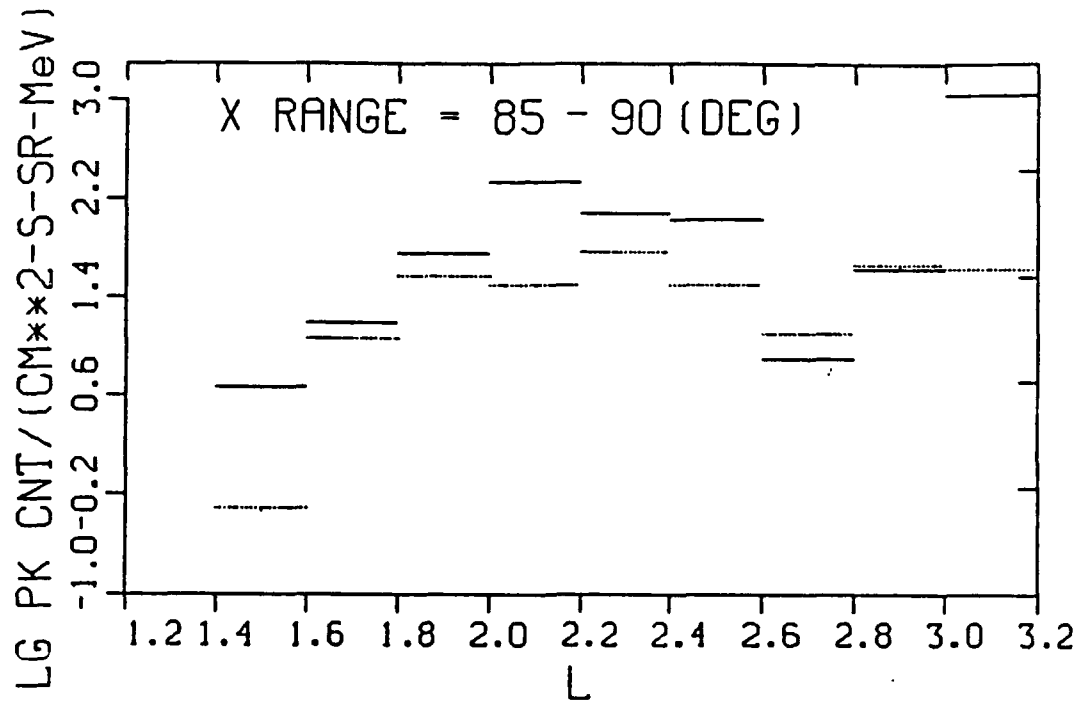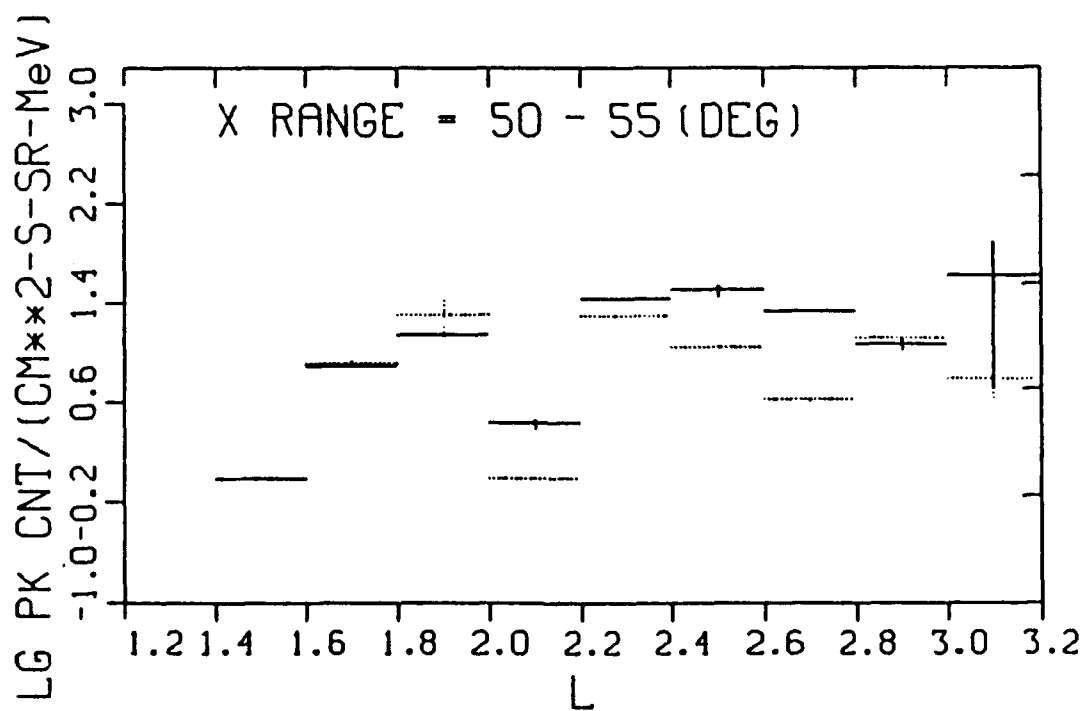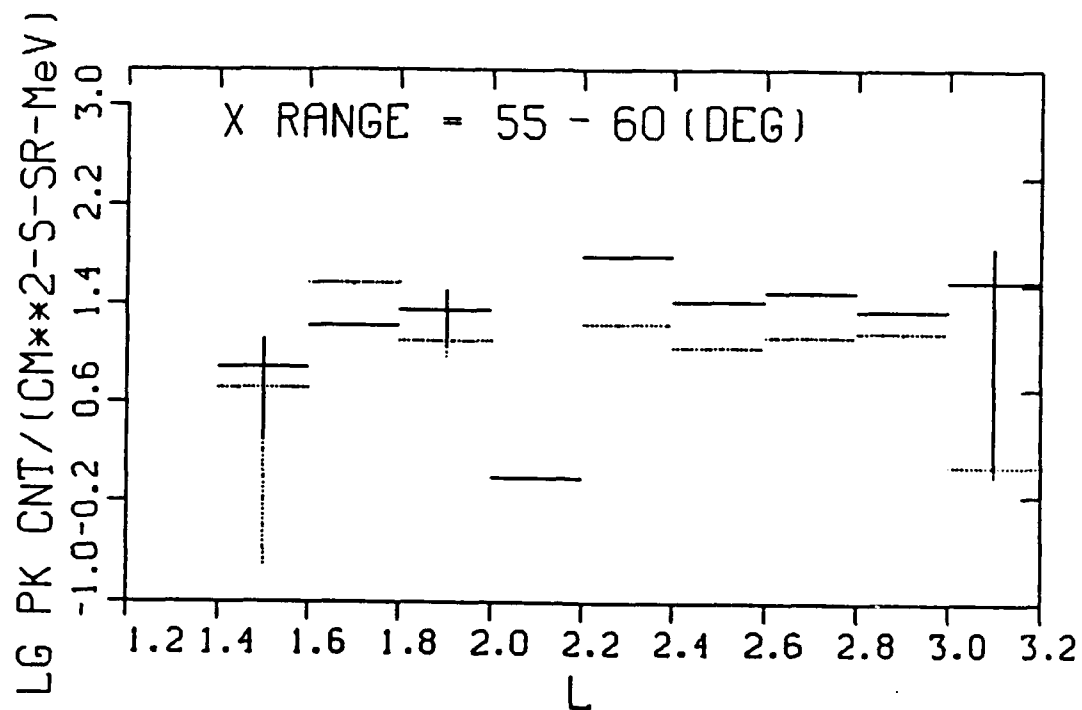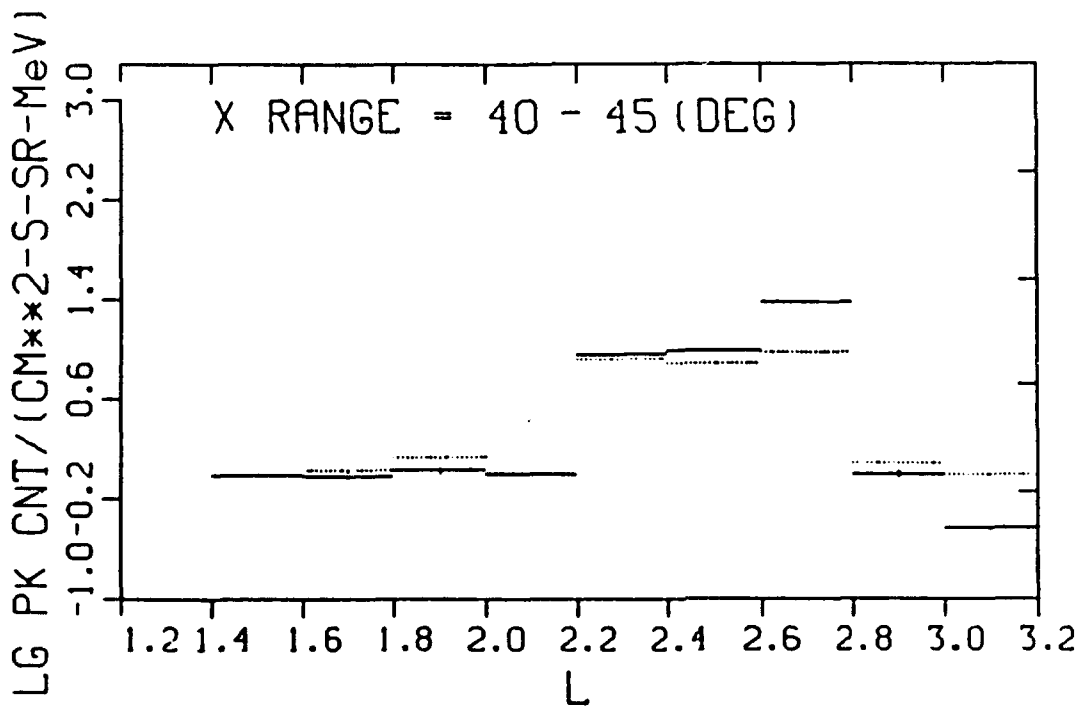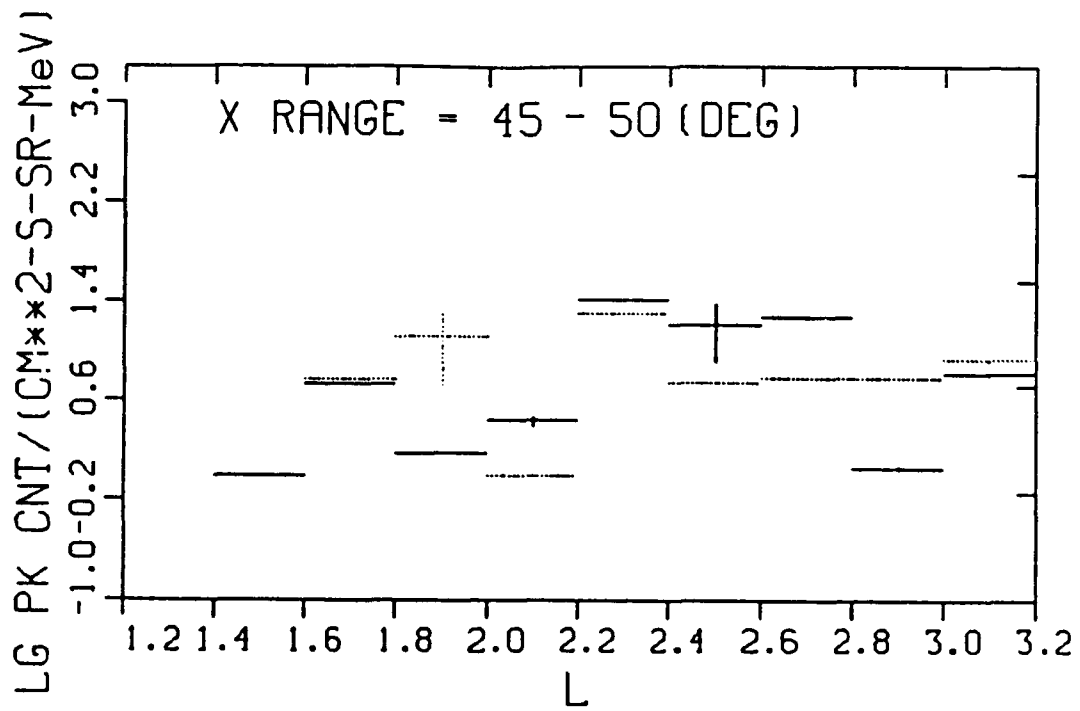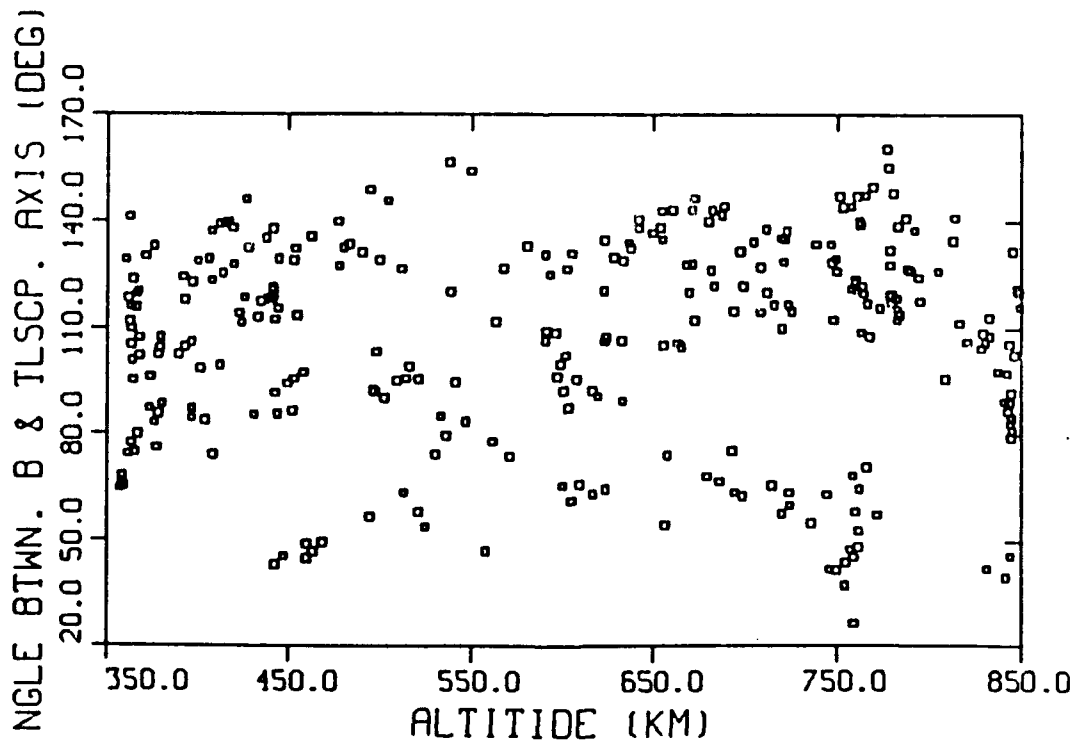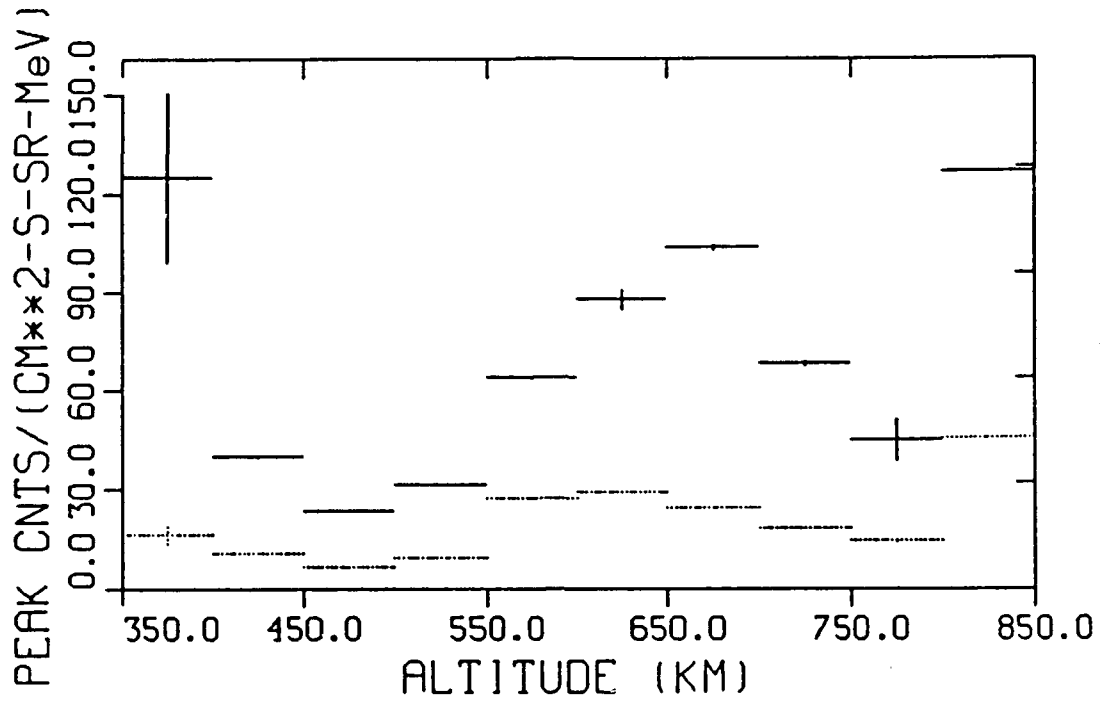
Figures 11a and 11b
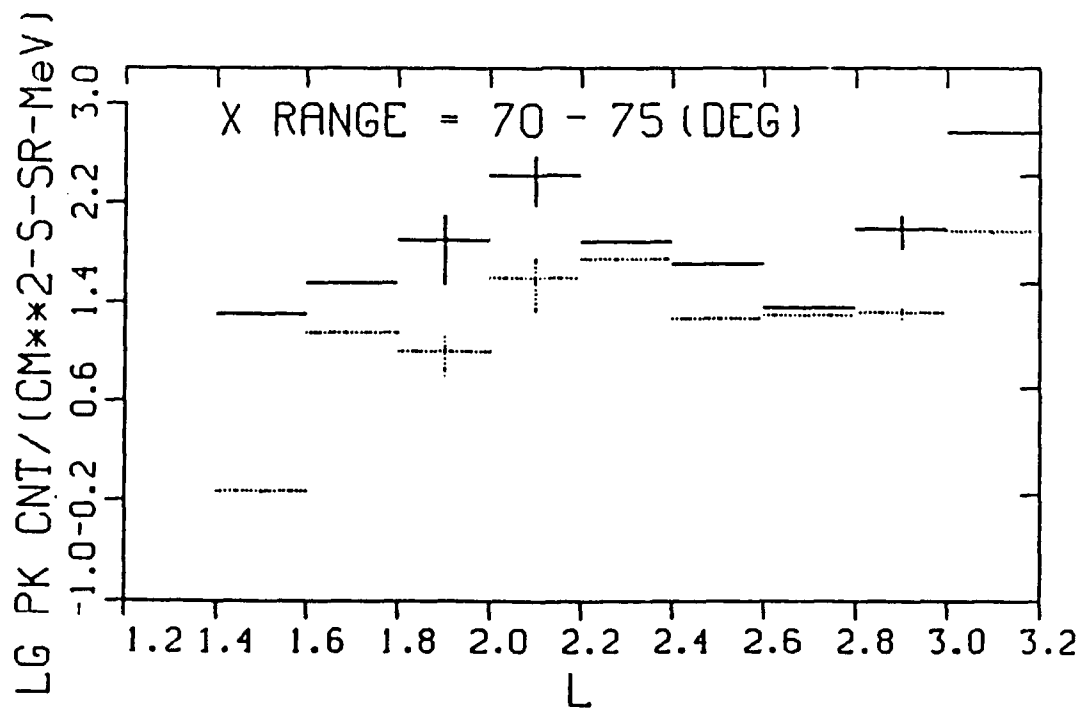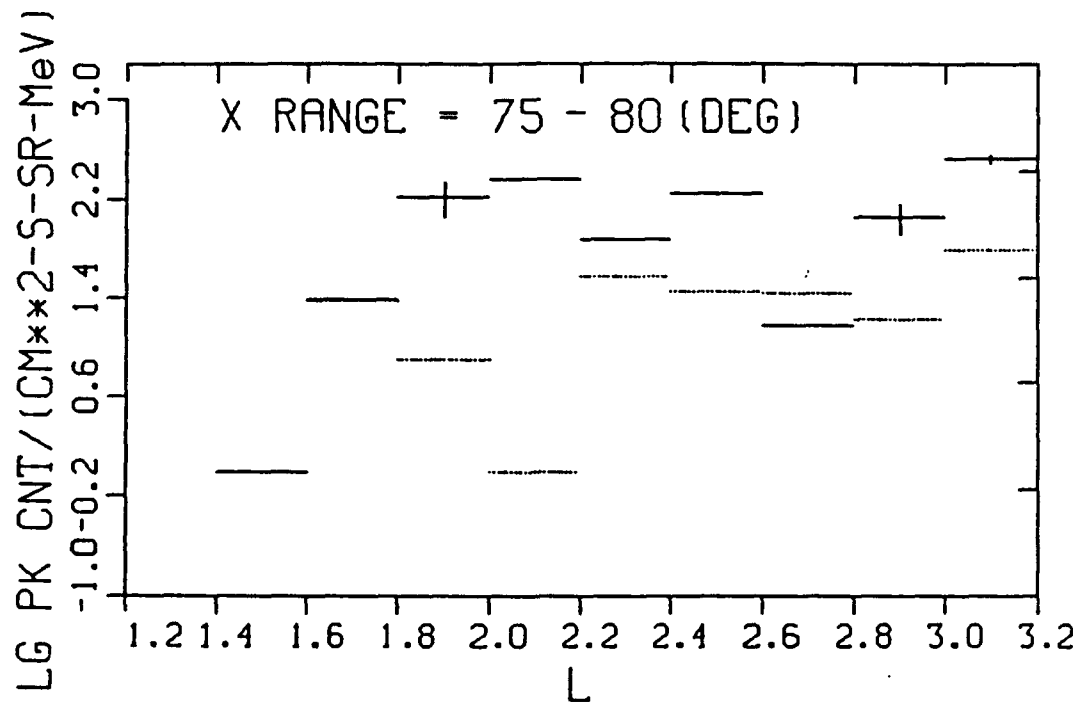
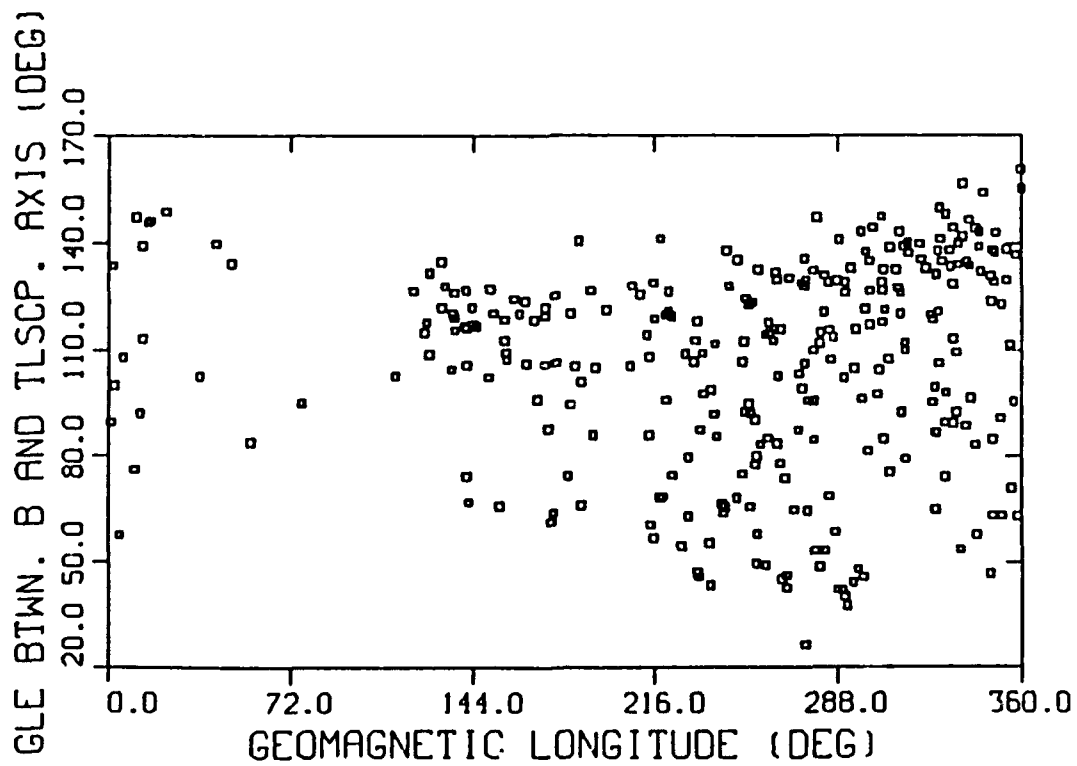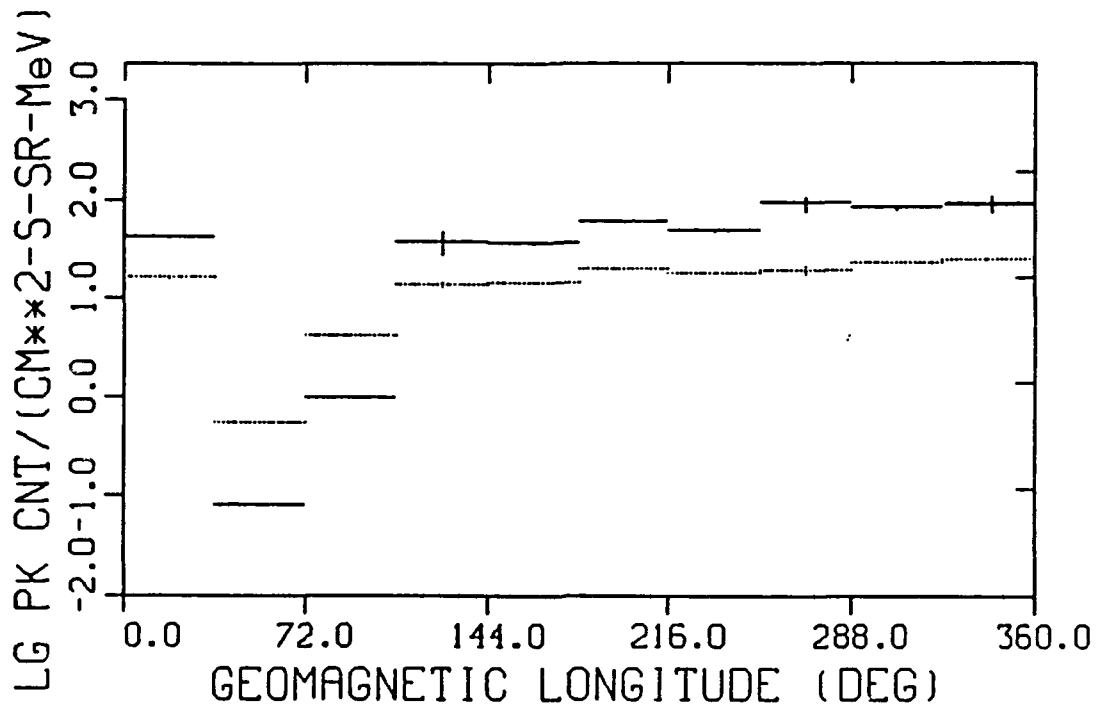Figures 12a and 12b
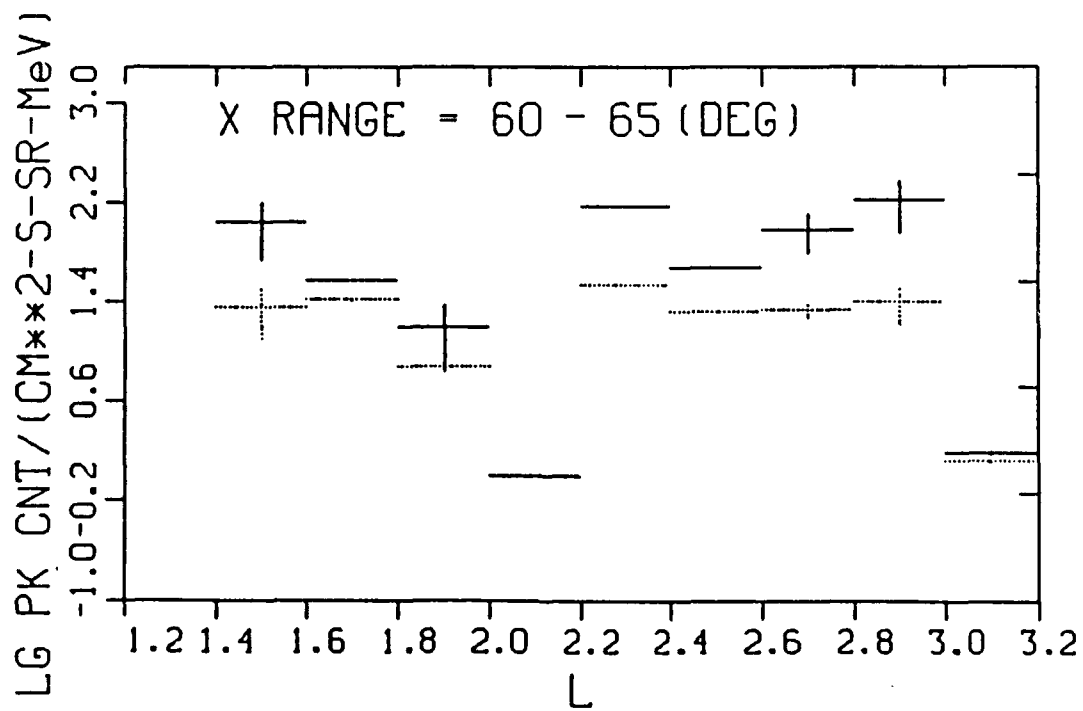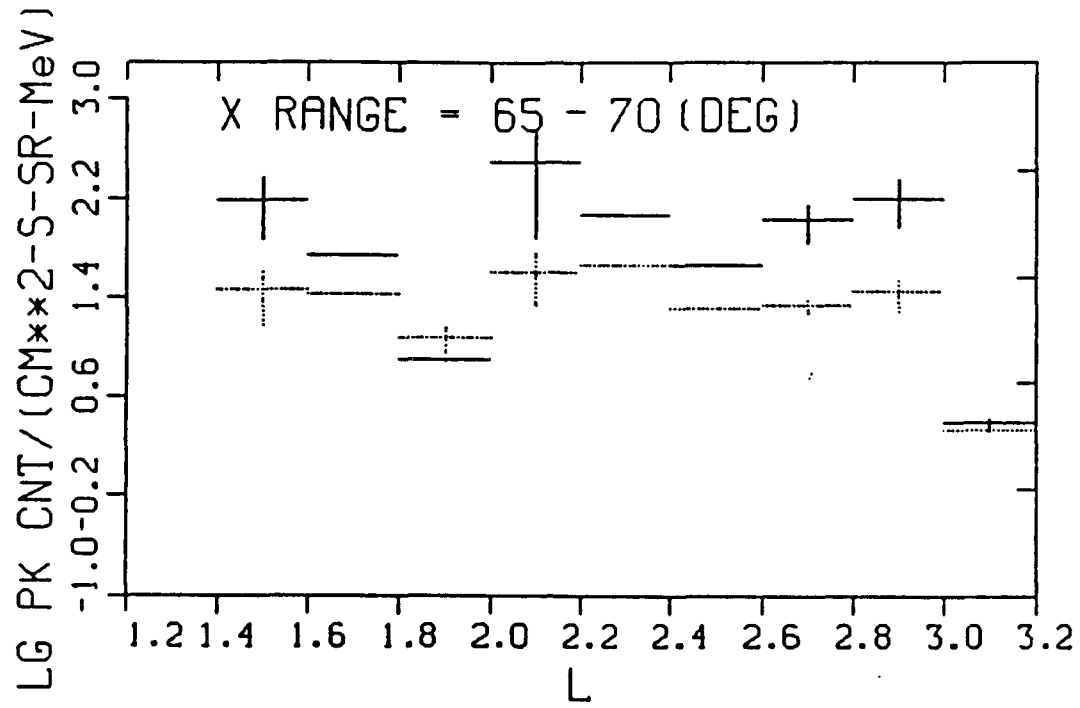
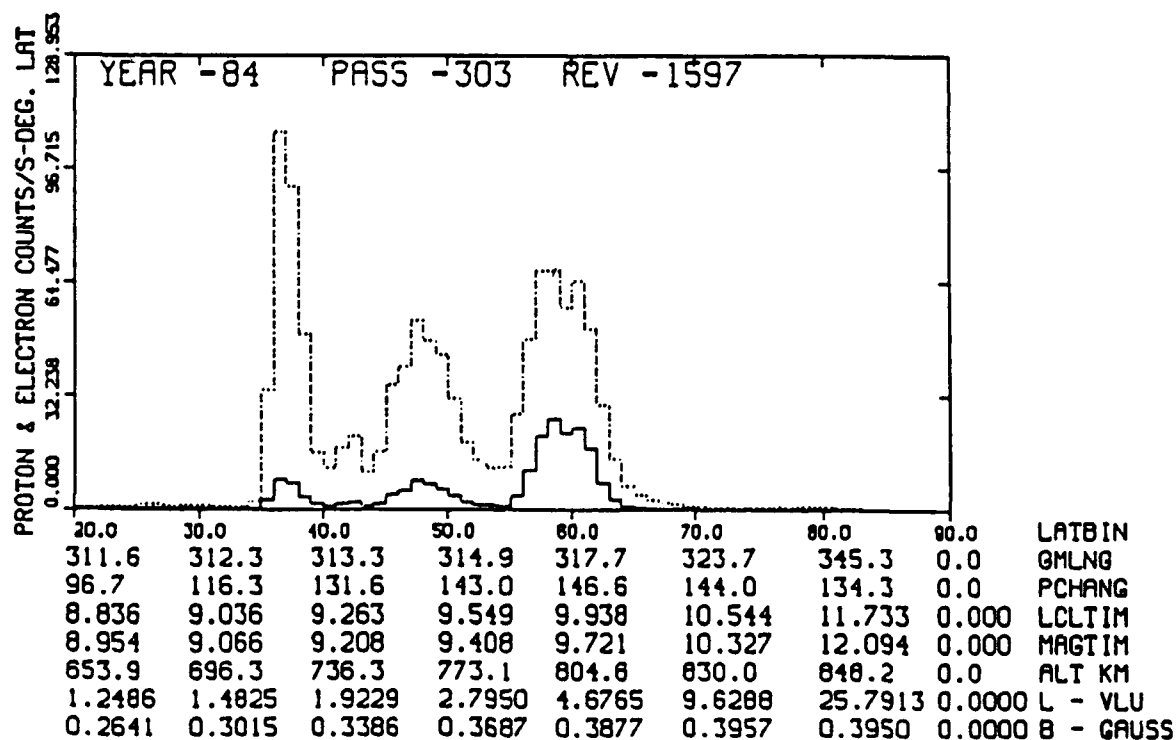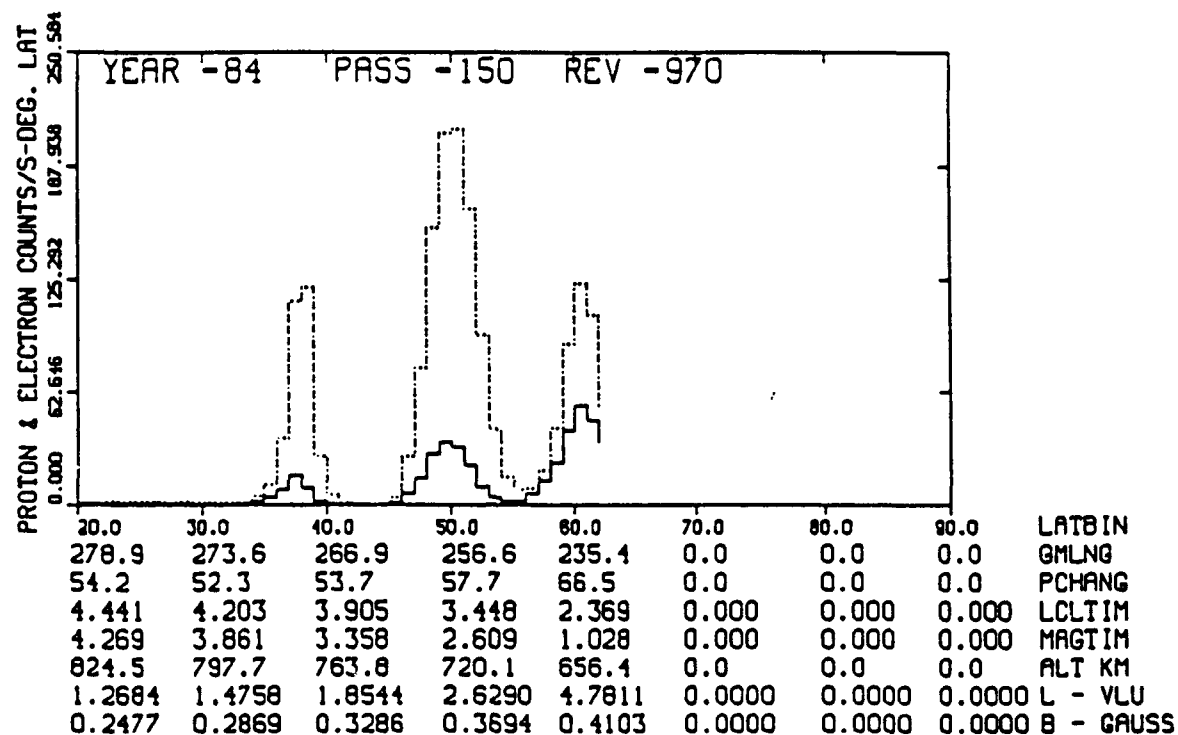Figures 13a and 13b

Figurs 14a and 14b

Figures 15a and 15b

Figures 16a and 16b

Figures 17a and 17b

Figures 18a and 18b

Local Time Effect-. Peak proton counting rates in the midlatitude region vs local time has been plotted in Fig. 19a, and the χ vs local time plotted in Fig. 19b. The reason for the low values of the peak counting rates in the local time range 10 - 14 hrs is due to the very high χ values ($\sim$ 130° - 160°) and consequently very low instrumental efficiency during these hours (vide Figs. 3a - 3f). It may be concluded that local time does not affect peak counting rates.

Seasonal Effect-. Monthly variations of both protons (dotted lines) and electrons (solid lines) are plotted in Fig. 20a. Lines along the zero flux value indicate absence of data points. Fluctuations of both proton and electron fluxes are very clearly seen. About the relative fluctuations of these fluxes, sometimes they overlap each other, and sometimes differ by a large amount. These effects seem to show repetitions. However, the bottom figure (Fig. 20b) illustrates that the repetitions of the relative variations of the maxima and minima of e and p fluxes are related to the χ angle or in other words to the instrumental efficiency; but the relative variations of the fluxes over a period of one month are a distinct effect.

III. C. Energy Spectra

The differential energy spectra of both electrons (solid lines) and protons (dotted lines) in the midlatitude region are shown in Figure 21. The proton spectra shows a knee at $\sim$ 1 MeV. These spectral shapes were common among previous observations which showed L dependent spectral shapes. Spectral shapes are also modulated by the minimum mirror altitude value of the particles. The spectral shapes may further be investigated for different L values and minimum mirror altitude ranges for further information.

IV. FUTURE PROJECTS

Quite a significant amount of study of the temporal and spatial features of the electrons and proton fluxes of the midlatitude zone lying to the North of the geomagnetic equator is done. In the northern part still remains to be conducted the for the low latitude zone and the auroral zone. Nothing has yet been done with the data of the global zones lying to the South of the equator. Regarding the completion of the project, the projected tasks are beyond the capacity of a single person (the PI) working a quarter time during regular semesters and full time during the summer terms, which totals less than 5 man-months ahead from now.
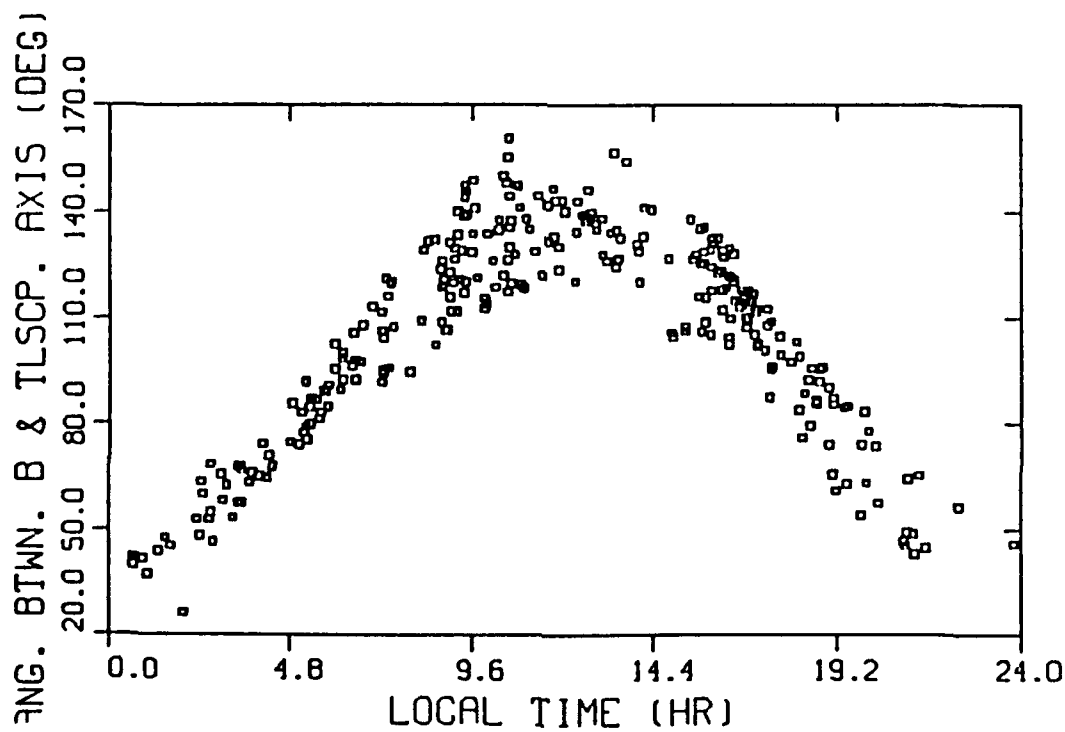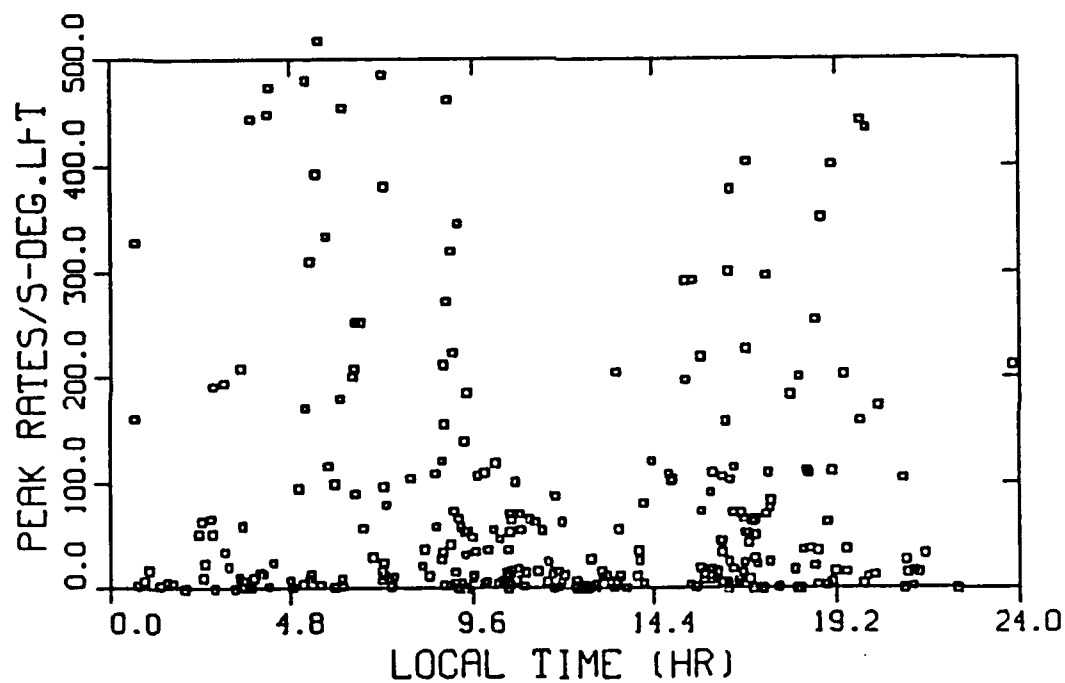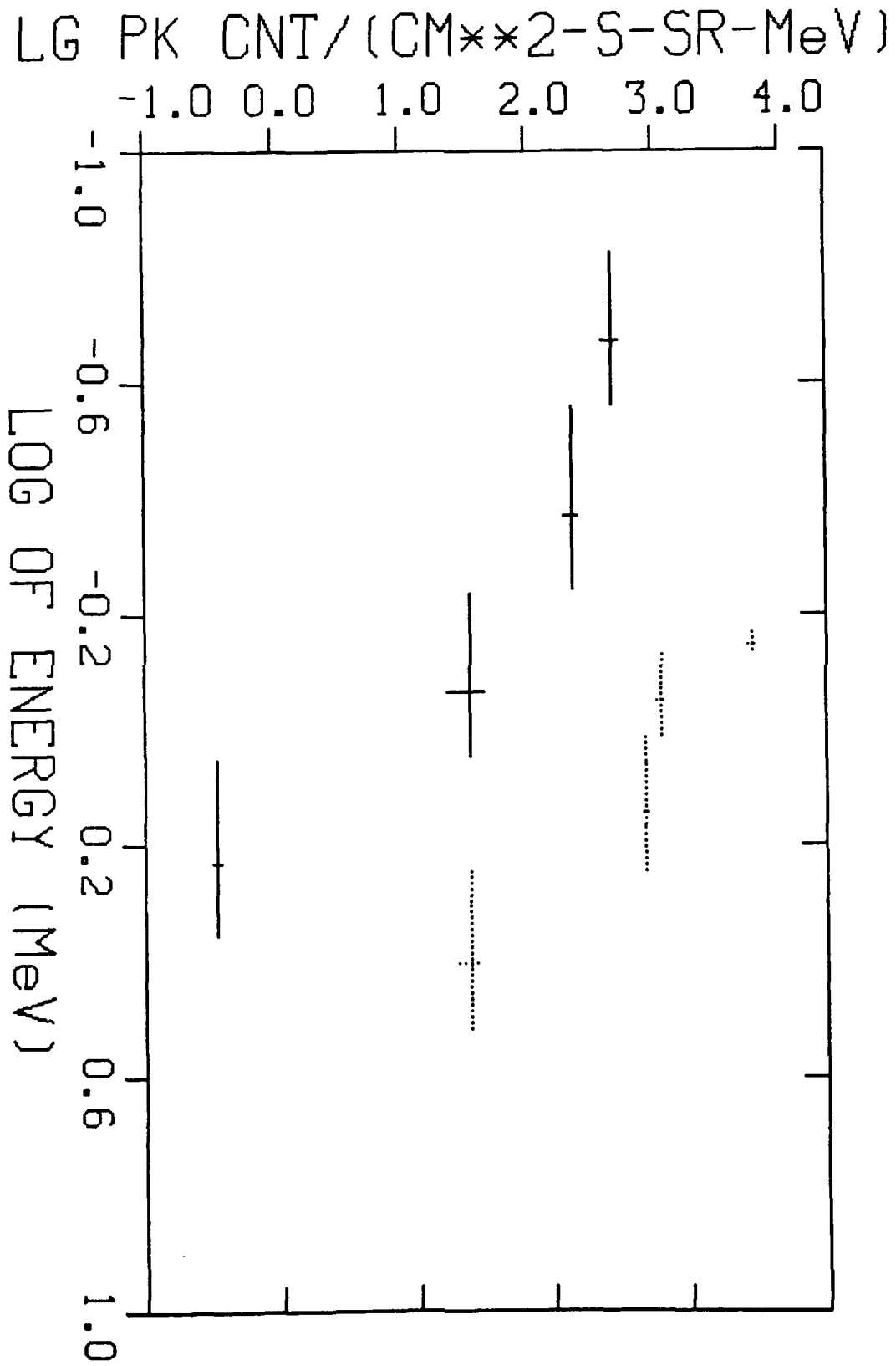
Figures 19a and 19b
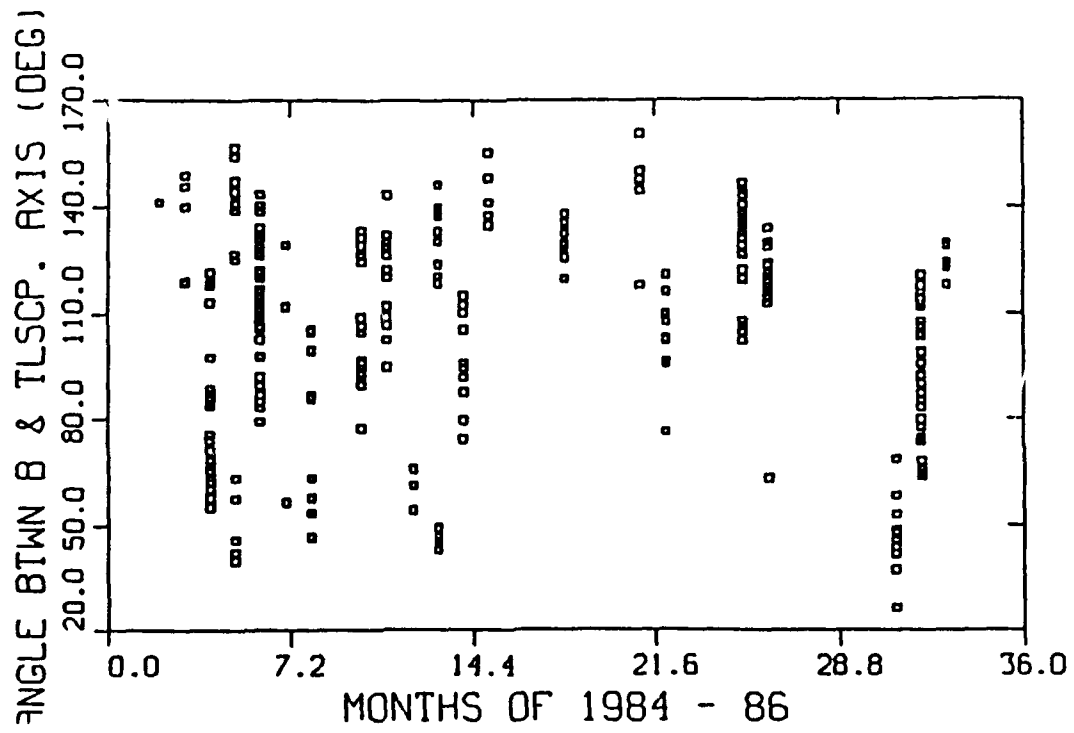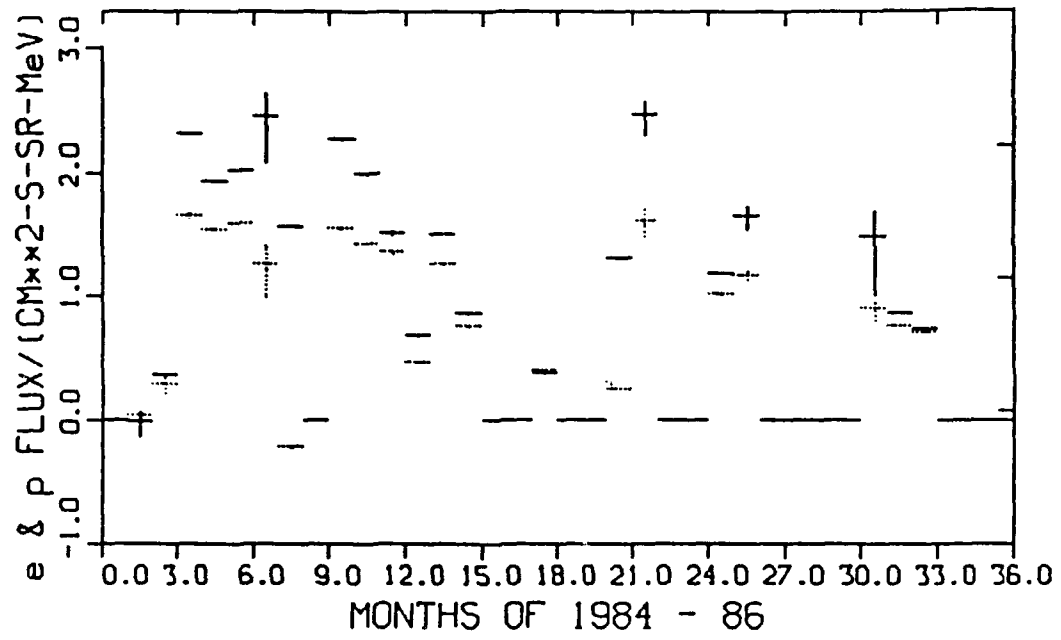
Figures 20a and 20b

Figure 21

V. PAPERS PUBLISHED, IN PRESS, AND PRESENTED

The following is a list of papers published, in press, submitted, and presented:

1. "Spatial and Temporal Variation of 0.65 - 35 MeV Protons and 0.19 - 3.2 MeV electrons in the Space Station Environment", published in the Journal of Geomagnetism and Geoelectricity.

2. "Solar-induced Variation of Proton Precipitation Near the Equator", in press for publication in the Journal of Atmospheric and Terrestrial Physics

3. "Solar Cycle Dependence of Proton Population Near the Equator", submitted for publication in the proceedings of Solar-Terrestrial Relationship Workshop held in May, 1992, in Ottawa, Canada.

4. An abstract on equatorial proton population published in EOS covering the abstracts for the Joint Spring meeting of AGU.

5. "Spatial and Temporal Features of 0.19 - 3.2 MeV electrons and 0.64 - 35 MeV protons", presented in the Western Pacific Geophysics meeting in Hong Kong during August 16 - 21, 1992.

6. "Significant Variation of Proton Population Near the Equator" was presented in the World Space Congress meeting in Washington, DC, during August 28 - September 7, 1992. The paper is still in the review process for consideration of publication in COSPAR journal.

VI. REFERENCES

Claffin, E. S., and R. S. White, A Study of Equatorial Inner Belt Protons, J. Geophys. Res., 79, 959, 1974.
Coffey, H., NOAA, Boulder, Colorado, Private Communication, 1992
Fahr, H. J., and B. Shizgal, Modern Exospheric Theories and Their Observational Relevance, Rev. of Geophys. Space Phys., 21, 75, 1983
Fischer, H. M., V. W. Auschart, and G. Wibberenz, Angular Distribution and Energy Spectra of Protons of Energy 5 $\leq E \leq 50$ MeV at the Lower Edge of the Radiation Belt in Equatorial Latitudes, J. Geophys. Res., 82, 537, 1977.
Hovestadt, D., B. Hausler, and M. Scholer, Observation of energetic particles at very low altitudes near the geomagnetic equator, Phys. Rev. Lett., 28, 1340, 1972.

Jacchia, L. G., Smithsonian Astrophysical Observatory Special Report, 377, Cambridge, Massachusetts, 1977.

Maher, L. J., Jr., J. Geophys. Res., 85, 4621, 1980

Miah, M. A., Observation of low energy particle precipitation at low altitude in the equatorial zone, J. Atmos. Terr. Phys., 51, 541, 1989.

Miah, M. A., Observation of $Z \geq 1$ particles below 300 km near the geomagnetic equator, J. Geomag. Geoelectr., 43, 461, 1991b.

Miah, M. A., Global peak flux profile of proton precipitation in the equatorial zone, Ind. J. Radio & Space Phys., 20, 127, 1991c.

Miah, M. A., Spatial and Temporal Features of Protons in Space Station Environment: Phoenix-1 Observations, Proc. 2nd Meeting of Space Consortium, 1992 (in press)

Miah, M. A., J. W. Mitchell, and J. P. Wefel, Magnetospheric particle detection efficiency of a conical telescope, Nucl. Instr. and Methods in Phys. Res., A281, 622, 1989.

Miah, M. A., T. G. Guzik, J. W. Mitchell, and J. P. Wefel, Phoenix-1 observation of equatorial zone particle precipitation, Genesis and Propagation of Cosmic Rays, eds. M. M. Shapiro and J. P. Wefel, D. Reidel Publishing Company, Dordrecht, p. 339, 1988.

Mizera, P. F., and J. B. Blake, Observations of ring current protons at low altitudes, J. Geophys. Res., 78, 1058, 1973.

Moritz, J., Energetic protons at low equatorial altitudes: A newly discovered radiation belt phenomenon and its explanation, Z. Geophys, 88, 701, 1972.

NOAA, Solar-Geophysical Data, July 1987, No. 515 (Supplement), Boulder, Colorado.

Parsignault, D. R., E. Holeman, and R. C. Filz, Long-Term Intensity Decrease in the 8- to 25-MeV Proton Fluxes at Low L Values, J. Geophys. Res., 86, 11,447, 1981.

Scholer, M., D. Hovestadt, and G. Morfill, Energetic He^+ Ions From the Radiation Belt at Low Altitudes Near the Geomagnetic Equator, 80, 80, 1975.